

# NONTHERMAL RADIATION OF YOUNG SUPERNOVA REMNANTS

V.N.Zirakashvili

*Pushkov Institute for Terrestrial Magnetism, Ionosphere and Radiowave Propagation, 142190, Troitsk,  
Moscow Region, Russia*

*Max-Planck-Institut für Kernphysik, Saupfercheckweg 1, 69117 Heidelberg, Germany*

F.A.Aharonian

*Dublin Institute for Advanced Studies, 31 Fitzwilliam Place, Dublin 2, Ireland*

*Max-Planck-Institut für Kernphysik, Saupfercheckweg 1, 69117 Heidelberg, Germany*

## ABSTRACT

A new numerical code, designed for the detailed numerical treatment of nonlinear diffusive shock acceleration, is used for modeling of particle acceleration and radiation in young supernova remnants. The model is based on spherically symmetric hydrodynamic equations complemented with transport equations for relativistic particles. For the first time, the acceleration of electrons and protons by both forward and reverse shocks is studied through detailed numerical calculations. We model the energy spectra and spatial distributions of nonthermal emission of the young supernova remnant RX J1713.7-3946 and compare the calculations with the spectral and morphological properties of this object obtained in broad energy band from radio to very high energy gamma-rays. We discuss the advantages and shortcomings of the so-called hadronic and leptonic models which assume that the observed TeV gamma-ray emission is produced by accelerated protons and electrons, respectively. We discuss also a "composite" scenario when the gamma-ray flux from the main parts of the shell has inverse Compton origin, but with a non-negligible contribution of hadronic origin from dense clouds interacting with the shell.

*Subject headings:* cosmic rays– acceleration– instabilities

## 1. Introduction

The paradigm of the diffusive shock acceleration (DSA) of relativistic particles (Krymsky 1977, Axford et al. 1977, Bell 1978, Blandford & Ostriker 1978) is generally accepted as the most likely scenario of production of galactic cosmic rays (CR) in supernova remnants (SNRs). Over the last 30 years a significant progress has been achieved in the development of theoretical models and understanding of the basic features of DSA (see e.g. Malkov & Drury 2001 for a review). On the other hand, the recent detailed studies of spectral and morphological features of young SNRs, first of all in the X-ray and very-high-energy or TeV gamma-ray band, provide excellent observational mate-

rial for development of detailed numerical models of acceleration and radiation of relativistic electrons and protons in young SNRs. These observations generally confirm in general terms the predictions of DSA. In particular the synchrotron X-radiation observed from many young SNRs implies an existence of multi-TeV energy electrons which is naturally explained by DSA. The detection of TeV gamma-rays from SNRs, like Cas A, RX J1713.7-3946, Vela Jr., RCW 86 (see Aharonian et al. 2008 for a recent review) give a more direct and unambiguous information about the effective acceleration of particles, electrons and/or protons, in SNRs to energies exceeding 100 TeV. In spite of the high quality data obtained from these

SNRs and intensive theoretical and phenomenological studies, we cannot yet firmly distinguish between two competing processes of gamma-ray production: the inverse Compton (IC) scattering of the background electromagnetic radiation by accelerated electrons (leptonic model) or a decay of neutral pions, mainly produced by accelerating protons during the interaction with the gas of the remnant (hadronic model). It should be noted that this ambiguity concerns the interpretation of the origin of gamma-rays, rather than the question of acceleration of protons in general. The presence of multi-TeV electrons in the SNR shells most likely implies also acceleration of protons - not only because the DSA operates identically for both electrons and protons; the presence of larger amount of nonthermal protons is needed in any case for production of magnetohydrodynamic (MHD) turbulence in the vicinity of a supernova shock. This is a necessary condition for effective acceleration of particles via DSA (see Malkov & Drury 2001 for a review).

In this paper we conduct detailed study acceleration of electrons and protons with an emphasis on the spectral and morphological features of high energy radiation produced by these particles in young supernova remnants. For that purpose we use a new numerical code of nonlinear diffusive shock acceleration developed by one of us in collaboration with V. Ptuskin (Zirakashvili & Ptuskin 2009). This model can be considered as a natural development of existing numerical codes (see e.g. Berezhko et al. 1994, Kang et al 2006), with new additional elements which despite their strong impact on the overall picture of acceleration in general, and on the properties of high energy radiation of SNRs in particular, have been ignored in the past. Namely, in our treatment, the solution of spherically symmetric hydrodynamic equations is combined with the energetic particle transport and acceleration by the *forward* shock (FS) and *reverse* shock (RS). Nonlinear response of energetic particles via their pressure gradient results in self-regulation of acceleration efficiency. To our knowledge, this is the first study in which the modification of the reverse shock and the nonthermal radiation related to the reverse shock is taken into account. The detailed calculations of radio, X-ray, gamma-ray emission components conducted within a self-consistent treatment of particle ac-

celeration by both forward and reverse shocks allows direct comparison of the observed spectral and morphological features with the model predictions. The inclusion of the radiation components related to the reverse shock seems to us a rather obligatory condition, given the effective acceleration of particles at the reverse shock to very high energies, as it is demonstrated in this paper. In this regard we note that the parameters characterizing the reverse shock can be significantly different in comparison with the parameters at the forward shock. As a result, the properties of radiation components from the reverse and forward shocks can be also significantly different. In particular the density of plasma and the magnetic field in the reverse shock can be very low which would dramatically increase the contribution of the IC component compared to the hadronic ( $\pi^0$ -decay) component of gamma-rays. Because of the higher gas density and stronger magnetic field, in the forward shock one may expect an opposite relation between the contributions of the electrons and protons to the high energy gamma-radiation.

The results of this study have a general character and can be applied to different young SNRs. In order to demonstrate their astrophysical implication, in this paper we apply the model to the supernova remnant RX J1713.7-3946 - the brightest and best studied TeV gamma-ray source among known shell-type supernova remnants (Aharonian et al. 2007a). The high quality gamma-ray and X-ray images and energy spectra available for this source make it a kind of template source for theoretical studies. On the other hand, this source have quite unusual radiation features (e.g. a lack of thermal X-radiation, a very low intensity of the synchrotron radio emission, etc.) so the conclusions derived for this source cannot be directly extended to other SNRs.

The paper is organized as follows. In Section 2 we briefly summarize the observational information about the supernova remnant RX J1713.7-3946. The short description of the model and basic features of accelerated particles is given in Section 3. The results of modeling of the broad-band emission radiation produced in hadronic and leptonic scenarios are presented and discussed in Sections 4, 5 and 6. In Section 7 we compare the magnetic field amplification and the maximum particle energies achieved in forward and reverse shocks. Fi-

nally, in Sections 8 and 9 we discuss and summarize the obtained results.

## 2. Observational properties of RX J1713.7-3946

The shell-type SNR RX J1713.7-3946 was discovered in X-rays during the ROSAT All-Sky Survey (Pfeffermann & Aschenbach 1996). The following observations of ASCA, Chandra, XMM-Newton and Suzaku (Koyama et al. 1997, Uchiyama et al. 2003, Cassam-Chenaï et al. 2004, Hiraga et al. 2005, Takahashi et al. 2008, Tanaka et al. 2008) revealed that the X-ray emission predominantly consists of the synchrotron component without an indication of a thermal X-ray component at the level of sensitivity of these instruments. The Suzaku measurements (Tanaka et al. 2008) allowed accurate derivation of the broad-band X-ray spectrum of the source over two energy decades, from 0.4 keV to 40 keV. It is described by a power-law with a photon index  $\sim 2$  and a smooth cut-off around a few keV.

The remnant is close to the position of the guest star AD393 described in the ancient Chinese records (Wang et al. 1997). If this not an accidental coincidence, the age of the remnant should be close to 1600 years.

Using the association of the supernova remnant with nearby molecular clouds, different estimates of the distance to the source have been suggested:  $D = 6$  kpc (Slane et al. 1999),  $D = 1$  kpc (Fukui et al. 2003) and  $1.3 \pm 0.4$  kpc (Cassam-Chenaï et al. 2004).

The remnant was claimed to be detected in gamma-rays by the CANGAROO collaboration (Muraishi et al. 2000). Later, the observation with the HESS array of imaging atmospheric Cherenkov telescopes revealed indeed a bright TeV gamma-ray source with a shell-type morphology quite similar to the synchrotron X-ray image of the source (Aharonian et al. 2004). The energy spectrum measured over the interval from 0.3 TeV to 100 TeV is hard; it is characterized by a photon index  $\simeq 2$  with a break or a cutoff around 10 TeV (Aharonian et al. 2007a).

The remnant is rather faint in radio. The recent ATCA measurements at 1.4 GHz gave the radio-intensity  $22 \pm 2$  Jy from the whole remnant (Acero et al. 2009). The radio and X-ray images

clearly show also an inner shell (Ellison et al. 2001, Lazendic et al. 2004, Cassam-Chenaï et al. 2004, Hiraga et al. 2005, Acero et al. 2009) with an angular diameter 0.5 degrees while the angular diameter of the remnant is close to one degree. The inner shell in the radio and X-ray images can be naturally attributed to the reverse shock propagating in the supernova ejecta, assuming that the electrons are accelerated also at the reverse shock. This is likely to be the case of the supernova remnant Cas A (Helder & Vink 2008). Generally, the reverse shock is not treated as an efficient accelerator, because the magnetic field of ejecta might be very weak due to the large expansion factor of the exploded star. However, similar to the case of the forward shock, the magnetic field can be significantly amplified also at the reverse shock (see Ellison et al. 2005), for example, in the course of the nonresonant streaming instability introduced by Bell 2004.

Another probable explanation of the inner shell could be its association with a pulsar wind nebula. It is known that an active pulsar may produce a corresponding nebula in an expanding supernova ejecta (Chevalier 2005). The inner shell does contain the radio pulsar PSR J1713-3945 with a period  $P = 392$  ms, but the latter is located at a distance  $D = 4.3$  kpc. Also, the pulsar's current spin-down luminosity does not exceed  $10^{34}$  erg s<sup>-1</sup>. This power is too low to produce the inner shell. The shell contains also a central compact object 1WGA J1713.4-3949 which is presumably a neutron star related to the remnant (Lazendic et al. 2003, Cassam-Chenaï et al. 2004).

## 3. Nonlinear model of diffusive shock acceleration

Hydrodynamical equations for the gas density  $\rho(r, t)$ , gas velocity  $u(r, t)$ , gas pressure  $P_g(r, t)$ , and the equation for the quasi-isotropic CR momentum distribution  $N(r, t, p)$  in the spherically symmetrical case are given by

$$\frac{\partial \rho}{\partial t} = -\frac{1}{r^2} \frac{\partial}{\partial r} r^2 u \rho \quad (1)$$

$$\frac{\partial u}{\partial t} = -u \frac{\partial u}{\partial r} - \frac{1}{\rho} \left( \frac{\partial P_g}{\partial r} + \frac{\partial P_c}{\partial r} \right) \quad (2)$$

$$\begin{aligned}
\frac{\partial P_g}{\partial t} &= -u \frac{\partial P_g}{\partial r} - \frac{\gamma_g P_g}{r^2} \frac{\partial r^2 u}{\partial r} - (\gamma_g - 1)(w - u) \frac{\partial P_c}{\partial r} \\
\frac{\partial N}{\partial t} &= \frac{1}{r^2} \frac{\partial}{\partial r} r^2 D(p, r, t) \frac{\partial N}{\partial r} - w \frac{\partial N}{\partial r} + \frac{\partial N}{\partial p} \frac{p}{3r^2} \frac{\partial r^2 w}{\partial r} \\
&+ \frac{\eta_f \delta(p - p_f)}{4\pi p_f^2 m} \rho(R_f + 0, t) (\dot{R}_f - u(R + 0, t)) \delta(r - R_f(t)) \\
&+ \frac{\eta_b \delta(p - p_b)}{4\pi p_b^2 m} \rho(R_b - 0, t) (u(R_b - 0, t) - \dot{R}_b) \delta(r - R_b(t))
\end{aligned} \tag{3}$$

Here  $P_c = 4\pi \int p^2 dp v p N/3$  is the CR pressure,  $w(r, t)$  is the advective velocity of CRs,  $\gamma_g$  is the adiabatic index of the gas and  $D(r, t, p)$  is the CR diffusion coefficient. It was assumed that the diffusive streaming of CRs results in the generation of magnetohydrodynamic (MHD) waves. CR particles are scattered by these waves. That is why the CR advective velocity  $w$  may differ from the gas velocity  $u$ . Damping of these waves results in an additional gas heating. It is described by the last term in Eq. (3). Two last terms in Eq. (4) correspond to the injection of thermal protons with momenta  $p = p_f$ ,  $p = p_b$  and mass  $m$  at the fronts of the forward and reverse shocks at  $r = R_f(t)$  and  $r = R_b(t)$  respectively. The dimensionless parameters  $\eta_f$  and  $\eta_b$  determine the corresponding injection efficiency<sup>1</sup>.

The pressure of energetic electrons is neglected, i.e. the electrons are treated as test particles. The evolution of electron distribution is described by an equation similar to Eq.(4), but with additional terms describing synchrotron and IC losses.

CR diffusion is determined by magnetic inhomogeneities. Strong streaming of accelerated particles changes medium properties in the shock vicinity. In particular, the CR streaming instability in young SNRs results in a high level of MHD turbulence (Bell 1978) and even in amplification of magnetic field (Bell 2004). Due to this effect the protons can be accelerated to energies beyond the so-called Lagage and Cesarsky limit,  $E \leq 100$  TeV (Lagage & Cesarsky 1983).

According to the recent numerical modeling of this instability, the magnetic field is amplified by the flux of run-away highest energy particles in the relatively broad region upstream of the shock (Zirakashvili & Ptuskin 2008). Magnetic energy density is a small fraction ( $\sim 10^{-3}$ ) of the energy density of accelerated particles. This amplified almost isotropic magnetic field can be considered as a large-scale magnetic field for lower energy particles which are concentrated in the narrow region upstream of the shock. Streaming instability of these particles produces MHD waves propagating in the direction opposite to the CR gradient. This gradient is negative upstream of the forward shock and MHD waves propagate in the positive direction.

We apply a finite-difference method to solve numerically Eqs. (1-4) upstream and downstream of the forward and reverse shocks. The auto-model variables  $\xi_1 = r/R_f(t)$  and  $\xi_4 = r/R_b(t)$  are used instead of the radius  $r$  upstream of the forward shock at  $r > R_f$  and upstream of the reverse shock at  $r < R_b$  respectively. The gases compressed at forward and reverse shocks are separated by a contact discontinuity (CD) at  $r = R_c$  that is situated between the shocks. We use variables  $\xi_2 = (r - R_c)/(R_f - R_c)$  and  $\xi_3 = (r - R_c)/(R_c - R_b)$  instead of  $r$  between the shocks downstream of the forward and reverse shocks, respectively.

A non-uniform numerical grid upstream of the shocks at  $r > R_f$  and  $r < R_b$  allows to resolve small scales of hydrodynamical quantities appearing due to the pressure gradient of low-energy CRs. Eq. (4) for CRs was solved using an implicit finite-difference scheme. An explicit conservative TVD scheme (Trac & Pen 2003) for hydrodynamical equations (1-3) and uniform spatial grid were used between the shocks. These equations are solved in the upstream regions using an implicit finite-difference scheme.

The magnetic field plays no dynamical role in the model. Since we do not model the amplification and transport of magnetic field here, its coordinate dependence should be specified for determination of cosmic ray diffusion and for calculation of synchrotron emission and losses. We shall assume below that the coordinate dependencies of the magnetic field and the gas density coincide up-

<sup>1</sup>Throughout the paper we use the subscripts "f" and "b" to the parameters characterizing the forward and reverse (backward) shocks, respectively.

stream and downstream of the forward shock:

$$B(r) = \sqrt{4\pi\rho_0} \frac{\dot{R}_f \rho}{M_A^f \rho_0}, \quad r > R_c. \quad (5)$$

Here  $\rho_0$  is the gas density of the circumstellar medium. The parameter  $M_A^f$  is similar to the Alfvén Mach number of the shock and determines the value of the amplified magnetic field strength. The magnetic energy downstream of the shock is estimated to be several percents of the dynamical pressure  $\rho_0 \dot{R}^2$  as was derived from the width of X-ray filaments in young SNRs (Völk et al. 2005). The characteristic range of this parameter is  $M_A^f \sim 10 \div 40$ . For example, the energy of the magnetic field of about 3.5 percent of the dynamical pressure (Völk et al. 2005) and characteristic compression ratio of a modified shock  $\sigma = 6$  correspond to  $M_A^f \approx 23$ . Since the plasma density  $\rho$  decreases towards the contact discontinuity downstream of the forward shock, the same is true for the magnetic field strength according to Eq. (5). This seems reasonable because of a possible magnetic dissipation in this region.

Situation is different downstream of the reverse shock at  $R_b < r < R_c$ . The plasma flow is as a rule strongly influenced by the Rayleigh-Taylor instability that occurs in the vicinity of the contact discontinuity and results in generation of MHD turbulence in this region. We assume that the magnetic field does not depend on radius downstream of the reverse shock while the dependence in the upstream region is described by the equation similar to Eq. (5):

$$B(r) = \sqrt{4\pi\rho_m} \frac{|\dot{R}_b - u(r_m)|}{M_A^b} \times \begin{cases} 1, & r < r_m, \\ \rho/\rho_m, & r_m < r < R_b, \\ \rho(R_b + 0)/\rho_m, & R_b < r < R_c \end{cases} \quad (6)$$

Here  $r_m < R_b$  is the radius where the ejecta density has a minimum and equals  $\rho_m$ . This radius  $r_m$  is generally close to the reverse shock radius  $R_b$  and is equal to it if the reverse shock is not modified by the cosmic ray pressure.

CR advective velocity may differ from the gas velocity on the value of the radial component of the Alfvén velocity  $V_{Ar}$  calculated in the isotropic random magnetic field:  $w = u + \xi_A V_{Ar}$ . Here

the factor  $\xi_A$  describes the possible deviation of the cosmic ray drift velocity from the gas velocity. Using Eq. (5) we obtain

$$w = u + \xi_A \frac{\dot{R}_f}{M_A^f} \sqrt{\frac{\rho}{3\rho_0}}, \quad r > R_c \quad (7)$$

The similar expression for the cosmic ray drift velocity is used upstream of the reverse shock at  $r < R_b$ . We use values  $\xi_A = 1$  and  $\xi_A = -1$  upstream of the forward and reverse shocks respectively, where Alfvén waves are generated by the cosmic ray streaming instability and propagate in the corresponding directions. The damping of these waves heats the gas upstream of the shocks (see McKenzie & Völk 1982) and limits the total compression ratios by a number close to 6. In the downstream region of the forward and reverse shock at  $R_b < r < R_f$  we put  $\xi_A = 0$  and therefore  $w = u$ .

Here we use the energy dependence of the CR diffusion coefficient like in the case of Bohm diffusion:  $D = \eta_B D_B$  calculated for the magnetic field radial dependencies given by Eq. (5) and (6). The parameter  $\eta_B$  describes the possible deviations of diffusion coefficient from the one achieved in the regime of Bohm diffusion,  $D_B = v_{pc}/3qB$ . Since the highest energy particles are scattered by small-scale magnetic fields, their diffusion is faster than the Bohm diffusion (Zirakashvili & Ptuskin 2008). The same is true for low energy particles because they can be resonantly scattered only by a fraction of the magnetic spectrum. Throughout the paper we use the value  $\eta_B = 2$ .

In real situations the level of MHD turbulence drops with distance upstream of the shock, so the diffusion could be quite fast there. The characteristic diffusive scale of highest energy particles is a small fraction  $\xi_0 \ll 1$  of the shock radius (see Zirakashvili & Ptuskin 2008) and is determined by the generation and transport of MHD turbulence in the upstream region (see also Vladimirov et al. 2006, Amato & Blasi 2006). The value  $\xi_0 \sim \ln^{-1}(D_c/D_s)$  is determined by ratio of diffusion coefficient  $D_c$  in the circumstellar medium and diffusion coefficient  $D_s \ll D_c$  in the vicinity of the shock. The MHD turbulence is amplified exponentially in time before the shock arrival from the background level by cosmic ray streaming instability. Since this process is not modelled here, we simply multiply the CR diffusion coefficient

cient  $D$  to the additional factor  $\exp((\xi_1 - 1)/\xi_0)$  upstream of the forward shock and to a similar factor  $\exp((1 - \xi_4)/\xi_0)$  upstream of the reverse shock. The characteristic range of  $\xi_0$  is  $0.05 \div 0.1$  (Zirakashvili & Ptuskin 2008).

It is believed that the supernova ejecta has some velocity distribution  $P(V)$  just after the supernova explosion (e.g. Chevalier 1982)

$$P(V) = \frac{3(k-3)}{4\pi k} \begin{cases} 1, & V < V_{ej} \\ (V/V_{ej})^{-k}, & V > V_{ej}. \end{cases} \quad (8)$$

Here the index  $k$  characterizes the steep power-low part of this distribution. The radial distribution of ejecta density is described by the same expression with  $V = r/t$ . The characteristic ejecta velocity  $V_{ej}$  can be expressed in terms of energy of supernova explosion  $E_{SN}$  and ejecta mass  $M_{ej}$  as

$$V_{ej} = \left( \frac{10(k-5)E_{SN}}{3(k-3)M_{ej}} \right)^{1/2} \quad (9)$$

Figures 1-5 illustrate the numerical results that are obtained for the SNR shock propagating in the medium with hydrogen number density  $n_H = 0.09 \text{ cm}^{-3}$  and temperature  $T = 10^4 \text{ K}$ . The number density of helium nuclei  $0.1n_H$  was assumed. We use the ejecta mass  $M_{ej} = 1.5M_\odot$ , the energy of explosion  $E_{SN} = 2.7 \cdot 10^{51} \text{ erg}$  and the parameter of ejecta velocity distribution  $k = 7$ . These combination of these parameters is chosen to explain the obtained gamma-ray fluxes within the hadronic model of gamma-rays (see next Section).

The initial forward shock velocity is  $V_0 = 4.6 \cdot 10^4 \text{ km s}^{-1}$ . The injection efficiency is taken to be independent of time  $\eta_b = \eta_f = 0.01$ , and the injection momenta are  $p_f = 2m(\dot{R}_f - u(R+0, t))$ ,  $p_b = 2m(u(R_b-0, t) - \dot{R}_b)$ . The high injection efficiency results in significant shock modification already at early epochs of the SNR expansion while the thermal sub-shock compression ratio is close to 2.5. This is in agreement with calculations of collisionless shocks (Zirakashvili 2007) and are supported by radio-observations of young extragalactic SNRs (Chevalier 2006). In hadronic models of gamma-radiation of RX J1713.7-3946 the ratio of relativistic electrons to protons  $K_{ep}$  appears significantly lower compared to the observed ratio for galactic cosmic rays which is around 0.01 at 10 GeV. A possible explanation could be the dependence of the electron injection efficiency on

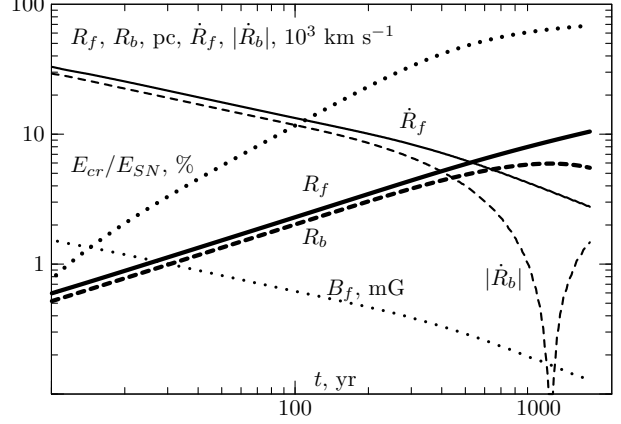


Fig. 1.— Time dependencies of parameters characterizing the forward and reverse shocks: the forward shock radius  $R_f$  (thick solid line), the reverse shock radius  $R_b$  (thick dashed line), the forward shock velocity  $\dot{R}_f$  (thin solid line); the reverse shock velocity  $\dot{R}_b$  (thin dashed line); the magnetic field strength downstream of the forward shock (thin dotted line); the ratio of the CR energy to the total energy of the supernova explosion  $E_{cr}/E_{SN}$  (dotted line).

the shock speed. In the paper we assume that the electron injection is inversely proportional to the square of the shock speed. Then the electron to proton ratio  $K_{ep} \sim 10^{-4}$  for a characteristic shock speed  $3000 \text{ km s}^{-1}$  of young SNRs corresponds to  $K_{ep} \sim 10^{-2}$  in the old SNRs with a characteristic shock speed  $300 \text{ km s}^{-1}$ . The old SNRs probably produce the main part of galactic GeV electrons.

The time evolution of the shock radii  $R_f$  and  $R_b$ , the forward and reverse shock speeds  $V_f = \dot{R}_f$  and  $V_b = \dot{R}_b$ , the CR energy  $E_{cr}/E_{SN}$  and the magnetic field strength  $B_f$  downstream of the forward shock are shown in Fig.1. The calculations were performed until the present epoch at  $t = 1620 \text{ yr}$ , when the forward shock speed drops down to  $\dot{R}_f = 2.76 \cdot 10^3 \text{ km s}^{-1}$  and the forward shock radius  $R_f = 10.5 \text{ pc}$  corresponding to the angular radius  $30'$  of the remnant RX J1713.7-3946, assuming 1.2 kpc distance to the source. At early epochs of SNR evolution the distance between reverse and forward shocks is only 10% of the remnant radius. Note that the automodel Chevalier-Nadezhin solution with  $k = 7$  predicts 23% thickness (Chevalier 1982). This can be attributed to the strong

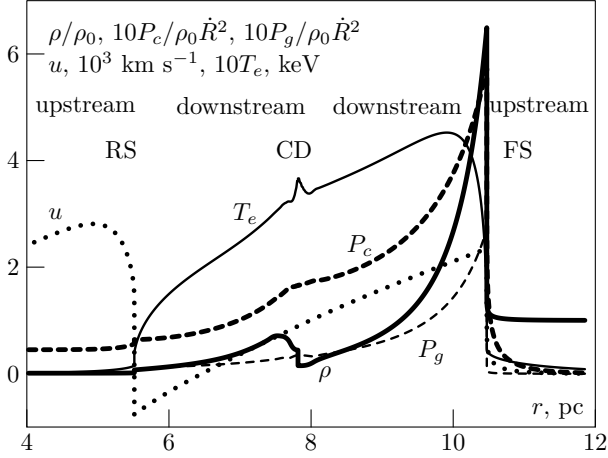


Fig. 2.— Radial dependencies of the gas density (thick solid line), the gas velocity (dotted line), CR pressure (thick dashed line), the gas pressure (dashed line) and the electron temperature (thin solid line) at  $t = 1620$  yr. The calculations result in the following parameters in the present epoch: the forward shock velocity  $2760 \text{ km s}^{-1}$ , its radius  $10.5 \text{ pc}$ , the magnetic field strength downstream of the forward shock  $127 \mu\text{G}$ . In the same figure we show the positions of the forward and reverse shocks, (FS and RS, respectively) and the contact discontinuity (CD).

modification of both shocks by CR pressure. The reverse shock is strongly decelerated only when the forward shock sweeps the gas mass comparable to the ejecta mass at  $t > 100 \text{ yr}$  and when the transition to the Sedov phase begins. It is important that the observable ratio  $R_b/R_f \sim 0.5$  is achieved at the Sedov phase when the forward shock speed is close to  $1/3$  of the characteristic ejecta speed  $V_{ej}$ . Since the synchrotron X-ray emission of SNR RX J1713.7-3946 extends well beyond  $1 \text{ keV}$ , the present forward shock speed cannot be significantly less than  $3 \cdot 10^3 \text{ km s}^{-1}$ . Therefore the characteristic velocity of the ejecta cannot be smaller than  $10^4 \text{ km s}^{-1}$ . Such high velocities may be attributed to Ib/c and IIb core collapse supernovae with low ejecta masses, but not to the most frequent core collapse IIP supernovae with characteristic ejecta velocities  $3 \cdot 10^3 - 4 \cdot 10^3 \text{ km s}^{-1}$  and high ejecta masses.

Radial dependencies of several key parameters at the present epoch  $t = 1620 \text{ yr}$  are shown in

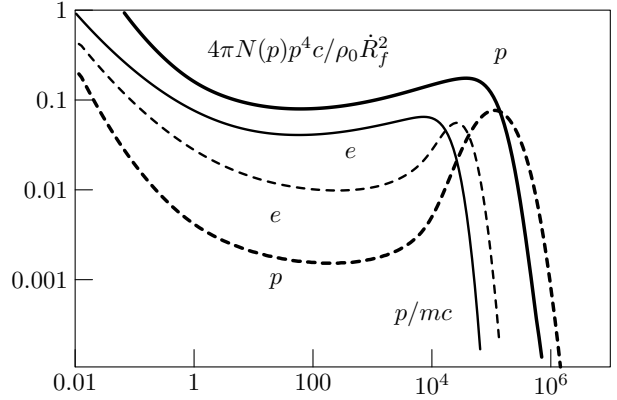


Fig. 3.— The energy distributions of accelerated protons (thick lines) and electrons (multiplied to the factor of 5000, thin lines) at the epoch  $t = 1620 \text{ yr}$ . The spectra at both the forward shock (solid lines) and at the reverse shock (dashed lines) are shown.

Fig.2. In the same figure we show the positions of the contact discontinuity and the forward and reverse shocks. The contact discontinuity between the ejecta and the interstellar gas is located at  $r = R_c = 7.8 \text{ pc}$ . The reverse shock in the ejecta is situated at  $r = R_b = 5.5 \text{ pc}$ . At the Sedov stage the reverse shock moves in the negative direction and reaches the center three thousand years after the supernova explosion. It should be noted that our one-dimensional calculations cannot adequately describe the development of the Rayleigh-Taylor instability of the contact discontinuity. In real situations the supernova ejecta and the circumstellar gas are mixed by turbulent motions in this region (see e.g. MHD modeling of Jun & Norman 1996).

In SNRs the plasma is heated to keV temperatures. The thermal X-ray emission is determined by the electron temperature. In young SNRs thermal electrons are not in equilibrium with protons if the temperature equilibration proceeds through the minimum available electron heating, i.e. through Coulomb collisions (Spitzer 1968). The evolution of electron temperature  $T_e$  is described by the following equation

$$\frac{\partial T_e}{\partial t} = -u \frac{\partial T_e}{\partial r} - \frac{2T_e}{3r^2} \frac{\partial r^2 u}{\partial r}$$

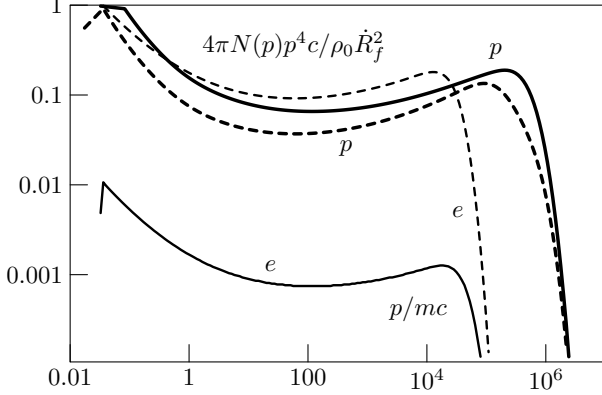


Fig. 4.— The energy distributions of accelerated protons (thick lines) and electrons (multiplied to the factor of 5000, thin lines) at  $t = 100$  yr. Spectra at both the forward shock (solid lines) and the reverse shock (dashed lines) are shown.

$$+ P_g \frac{8\sqrt{2}q^4}{3m_e m} \left( \frac{m_e}{T_e} \right)^{3/2} \lambda_{ep} \quad (10)$$

where  $\lambda_{ep} \sim 30$  is the Coulomb logarithm. The corresponding temperature is also shown in Fig.2.

Spectra of accelerated protons and electrons are shown in Fig.3. At the present epoch the maximum energy of protons accelerated in this SNR is about 140 TeV, while higher energy particles have already left the remnant. The spectra of both electrons and protons at the reverse shock show significant bumps just before the cut-offs. Because the reverse shock presently moves in the rarefied medium of the ejecta, the amount of freshly injected low-energy particles is relatively small, while many high energy particles accelerated earlier have not left the reverse shock yet, and continue to be accelerated.

The spectra for an early epoch,  $t = 100$  yr are shown in Fig.4. Since the shock speed was  $V_f = 1.3 \cdot 10^4 \text{ km s}^{-1}$ , the maximum energy of particles was also higher. For the forward shock it is about 650 TeV.

Spatially integrated proton and electron spectra at the present epoch  $t = 1620$  yr are shown in Fig.5. We also show the spectrum of run-away particles. These particles have already left the simulation domain through an absorbing boundary at  $r = 2R_f$ . The sum of the proton spectra shown is the total cosmic ray spectrum produced in this

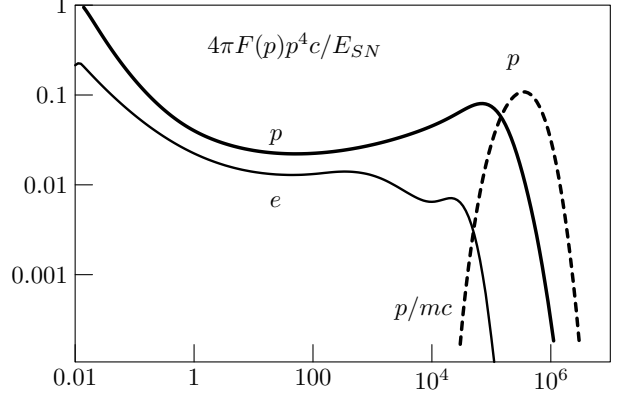


Fig. 5.— Spatially integrated spectra of accelerated protons (solid line) and electrons (multiplied to the factor of 5000, thin solid line) at  $t = 1620$  yr. Spectrum of run-away particles which have left the remnant is also shown (dashed line).

SNR over the last 1620 years after SN explosion. For this SNR, the spectrum of cosmic ray protons have a maximum at 800 TeV. This is somewhat smaller than the required value to explain the knee in the cosmic ray spectrum.

The results of calculations of radiation produced by accelerated electrons and protons are presented and discussed in the next sections. The gamma-ray spectra from proton-proton interactions are calculated using the formalism of Kelner et al. 2006. For calculations of IC gamma-rays we use standard expressions (see e.g. Blumenthal & Gould 1970). In calculations we take into account the target photons of the microwave background radiation only. We checked that other diffuse radiation fields do not contribute significantly to the gamma-ray production, unless the SNR is located in a regions with significantly (by an order of magnitude) enhanced optical and infrared radiation background. For calculations of synchrotron radiation we take into account that in real situations the magnetic field has some probability distribution  $P(B)$ . This makes the cut-off in the spectrum of synchrotron radiation somewhat smoother (see Appendix).

#### 4. Hadronic scenario

The results of calculations of the broad-band emission for the case of hadronic origin of high



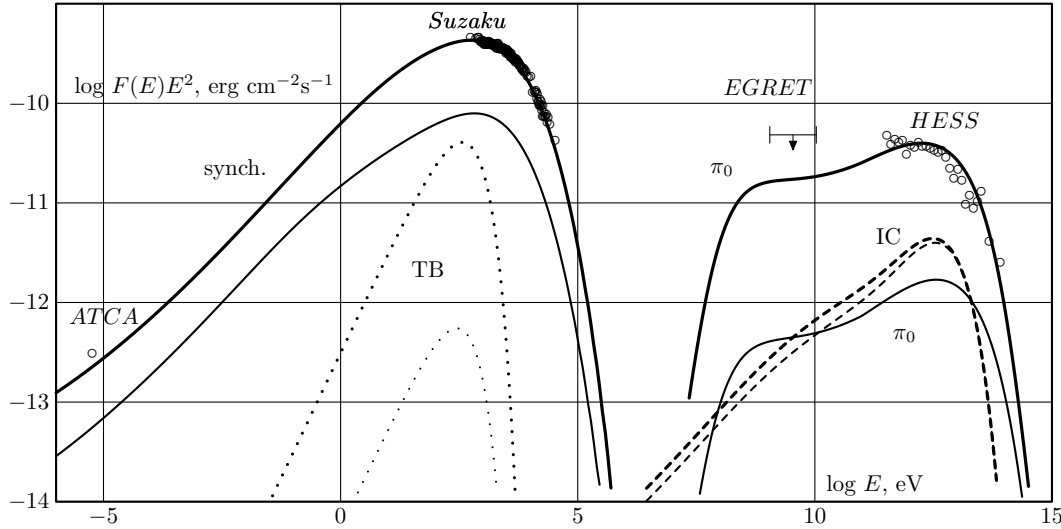


Fig. 6.— The results of modeling of nonthermal radiation of RX J1713.7-3946 within the hadronic scenario of gamma-ray production. The following basic parameters are used:  $t = 1620$  yr,  $D = 1.2$  kpc,  $n_H = 0.09$  cm $^{-3}$ ,  $E_{SN} = 2.7 \cdot 10^{51}$  erg,  $M_{ej} = 1.5 M_\odot$ ,  $M_A^f = M_A^b = 23$ ,  $\xi_0 = 0.05$ , the electron to proton ratios at the forward and reverse shocks  $K_{ep}^f = 10^{-4}$  and  $K_{ep}^b = 1.4 \cdot 10^{-3}$ . The calculations lead to the following values of the magnetic fields and the shock speeds at the present epoch: the magnetic field downstream of the forward and reverse shocks  $B_f = 127$   $\mu$ G and  $B_b = 21$   $\mu$ G respectively, the speed of the forward shock  $V_f = 2760$  km s $^{-1}$ , the speed of the reverse shock  $V_b = -1470$  km s $^{-1}$ . The following radiation processes are taken into account: synchrotron radiation of accelerated electrons (solid curve on the left), IC emission (dashed line), gamma-ray emission from pion decay (solid line on the right), thermal bremsstrahlung (dotted line). The input of the reverse shock is shown by the corresponding thin lines. Experimental data in gamma-ray (HESS; Aharonian et al. 2007a) and X-ray bands (Suzaku; Tanaka et al. 2008), as well as the radio flux  $22 \pm 2$  Jy at 1.4GHz (ATCA; Acero et al. 2009) from the whole remnant are also shown.

energy gamma-rays are shown in Fig.6. The principal model parameters used in calculations are described in the figure caption. Note that at the present epoch already 70 % of the explosion energy of  $2.7 \times 10^{51}$  erg has been transferred to accelerated protons (see Fig.1), most of them still confined in the shell of the remnant (see Fig.5). The maximum energies are 140 TeV and 23 TeV for protons and electrons respectively. Although the reverse shock contributes significantly to the highest energy particles, especially around 100 TeV (see Fig.3), the gamma-ray production related to this population of protons is suppressed because of the low density of the ejecta plasma. The contribution of electrons directly accelerated by the reverse shock to synchrotron radiation and IC gamma-rays is more significant. In particular, the reverse shock produces 16% of X-rays. Moreover, the bump at the end of IC spectrum is contributed

mostly by these electrons. The injection efficiency of electrons is adjusted in order to reproduce the total intensity of synchrotron X-rays. The electron injection efficiency at the reverse shock was adjusted to reproduce the observable radio-intensity of the inner ring. The gray scale radio images of Ellison et al. 2001 and Lazendic et al. 2004 were used in order to obtain a rough estimate of radio-flux 4 Jy at 1.4 GHz from this region. The modelled total radio flux is slightly below the observed flux. Note however that the space-integrated faint radio flux contains uncertainties, in particular the contribution of the background thermal radio emission can be quite significant.

In Fig.6 we show also the energy flux of the thermal bremsstrahlung. It has a maximum at 0.4 keV and approximately equals to the energy flux of gamma-rays produced in proton-proton interactions. Note that the ratio of the energy flux of the

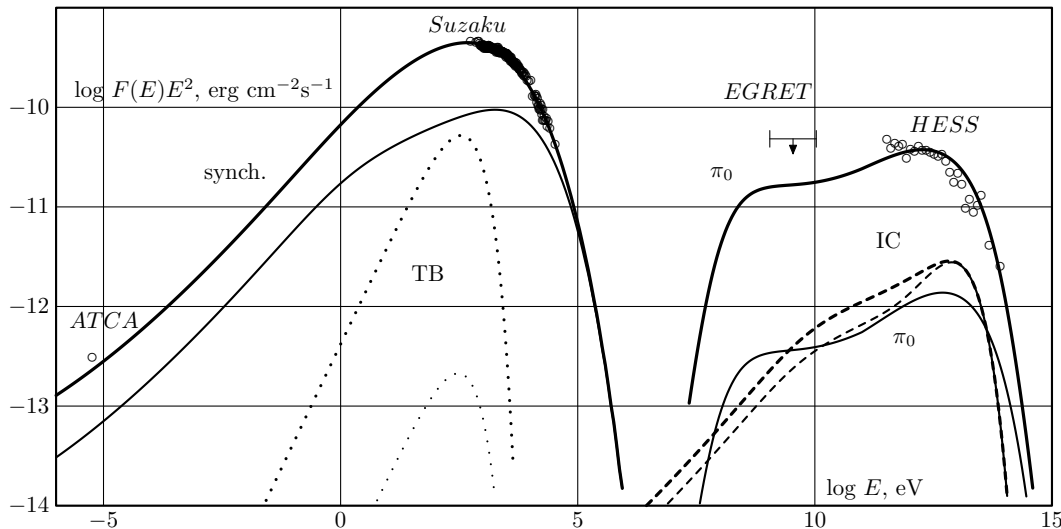


Fig. 7.— The same as in Fig.6, but for the supernova shock propagating in the medium with  $r^2$  density profile, assuming the following parameters  $t = 1620$  yr,  $D = 1.3$  kpc,  $E_{SN} = 2.5 \cdot 10^{51}$  erg,  $M_{ej} = 1.4 M_{\odot}$ ,  $M_A^f = M_A^b = 23$ ,  $\xi_0 = 0.05$ ,  $K_{ep}^f = 1.5 \cdot 10^{-4}$ ,  $K_{ep}^b = 4.4 \cdot 10^{-4}$ . The undisturbed hydrogen number density at the present shock position is  $n_H = 0.12 \text{ cm}^{-3}$ . The calculations lead to the following values of the magnetic fields and the shock speeds at the present epoch: the magnetic field downstream of the forward and reverse shocks  $B_f = 131 \mu\text{G}$  and  $B_b = 28 \mu\text{G}$ , respectively, the speed of the forward shock  $V_f = 2260 \text{ km s}^{-1}$ , the speed of the reverse shock  $V_b = -3010 \text{ km s}^{-1}$ .

thermal emission to the flux of "hadronic" gamma-rays does not depend on the density of ambient plasma, but depends on the shock speed and the cosmic ray acceleration efficiency (see Appendix).

It is expected that a circumstellar medium around progenitors of Ib/c and IIb supernova is strongly nonuniform. At the main sequence (MS) phase the stellar wind of progenitor creates rarefied bubble in the surrounding medium. Later the part of this bubble is filled with a dense gas ejected by progenitor at the Red Super Giant (RSG) phase of the stellar evolution. At the end of the progenitor evolution this gas most likely will be swept up and transported to the MS bubble periphery by a powerful Wolf-Rayet stellar wind. (see Chevalier 2005 for a review).

It seems that the corresponding MS bubble is indeed found. SNR RX J1713.7-3946 is surrounded by a massive shell of molecular gas (Fukui 2008). The densest cores of molecular gas (clouds C and D) are probably swept up by the forward shock of the SNR. This is the reason to consider the SNR evolution in the circumstellar medium with a positive density gradient. The results ob-

tained for the gas density profile proportional to the square of the radius are shown in Fig.7. A similar "bubble" model, but with a sharper density profile was considered by Berezhko & Völk 2006.

Results of calculations of the broad-band emission presented in Fig.7 are quite similar to the ones shown in Fig.6, however the agreement with observations is achieved with different set of model parameters. Also, note that in this case the reverse shock produces 35% of the total X-ray emission.

Note that in both cases the results are obtained for a low density gas. A similar number density close to  $n_H \sim 0.1 \text{ cm}^{-3}$  has been suggested by Morlino et al. 2008 in their hadronic models of gamma-emission of SNR RX J1713.7-3946. The low density gas is required also from the upper limit on the thermal X-ray emission from this supernova remnant (see e.g. Cassam-Chenaï et al. 2004, Takahashi et al. 2008, Tanaka et al. 2008) and is in agreement with a simple estimate of the gamma-ray intensity (see Appendix C). Significantly denser gas,  $n_H \sim 1 \text{ cm}^{-3}$ , was assumed by Berezhko & Völk 2006. This is because they

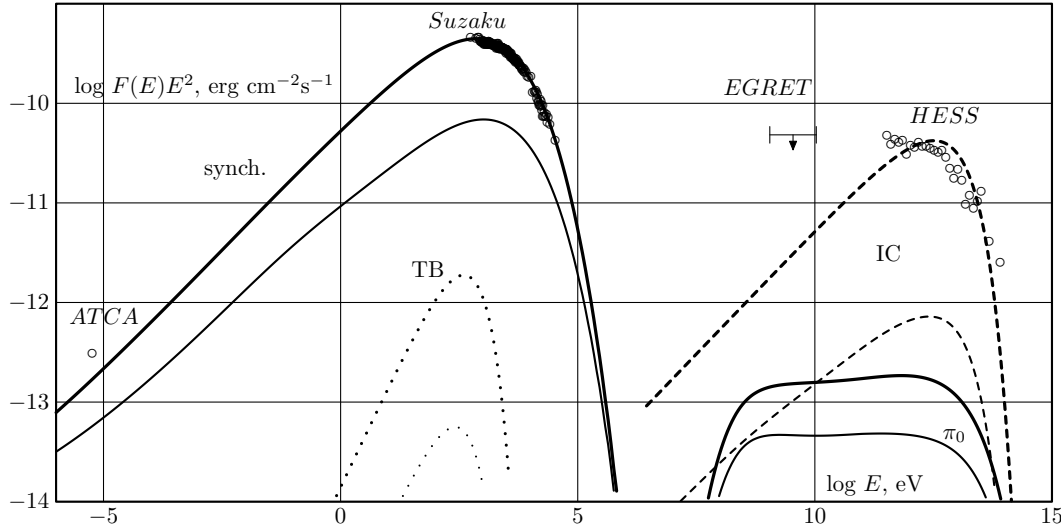


Fig. 8.— Broad-band emission of RX J1713.7-3946 for the leptonic scenario of gamma-rays with a non-modified forward shock. The principal model parameters are:  $t = 1620$  yr,  $D = 1.5$  kpc,  $n_H = 0.02$  cm $^{-3}$ ,  $E_{SN} = 1.2 \cdot 10^{51}$  erg,  $M_{ej} = 0.74 M_{\odot}$ ,  $M_A^f = 69$ ,  $M_A^b = 10$ ,  $\xi_0 = 0.1$ ,  $K_{ep}^f = 2.3 \cdot 10^{-2}$ ,  $K_{ep}^b = 9 \cdot 10^{-4}$ . The calculations lead to the following values of the magnetic fields and the shock speeds at the present epoch: the magnetic field downstream of the forward and reverse shocks  $B_f = 17$   $\mu$ G and  $B_b = 31$   $\mu$ G, respectively, the speed of the forward shock  $V_f = 3830$  km s $^{-1}$ , the speed of the reverse shock  $V_b = -1220$  km s $^{-1}$ . The following radiation processes are taken into account: synchrotron radiation of accelerated electrons (solid curve on the left), IC emission (dashed line), gamma-ray emission from pion decay (solid line on the right), thermal bremsstrahlung (dotted line). The input of the reverse shock is shown by the corresponding thin lines.

assumed that the cosmic ray acceleration occurs only at 1/5 part of the shock surface.

## 5. Leptonic scenario

The observed X-ray to gamma-ray energy flux ratio close to 15 determines the average value of the magnetic field  $B \sim 12$   $\mu$ G when the leptonic origin of gamma-emission in RX J1713.7-3946 becomes possible. How realistic is such a weak magnetic field?

The amplified magnetic fields can be quite weak if the SNR shock propagates in the rarefied medium. However since the magnetic field at the reverse shock is several times lower than the magnetic field at the forward shock (see previous Section) and the X-ray intensities of the shocks are comparable, the IC emission will be mainly produced at the reverse shock; this seems to be in conflict with HESS observations.

For this reason we consider a unmodified for-

ward shock of SNR. If the injection is not effective at the forward shock, the energy density of cosmic rays will be low and the same will be true for the amplified magnetic field. Such a situation is possible, in particular, for a perpendicular SNR shock propagating in the medium with an azimuthal magnetic field. In this case we use a very small injection parameter  $\eta_f = 10^{-5}$  at the forward shock and the standard value  $\eta_b = 10^{-2}$  for the injection parameter at the reverse shock. Thus in this scenario we deal with unmodified forward shock and modified reverse shock. Since, under these assumption, the electron to proton ratio  $K_{ep}$  is close to the observed ratio for galactic cosmic rays, 0.01 at 10 GeV, the electron injection was taken to be independent on the shock velocity. We also use a higher value  $M_A^f = 69$  for the forward shock, and adopt the distance  $D = 1.5$  kpc that is close to an upper limit according to Cassam-Chenaï et al. 2004 and Fukui 2008.

We should note that the shock speed is one of

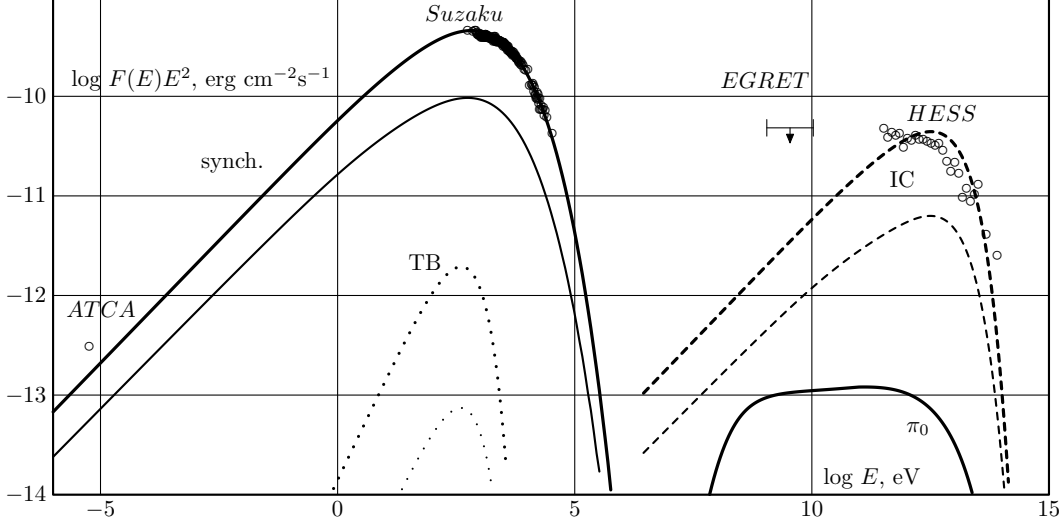


Fig. 9.— The same as in Fig.8 but for unmodified forward and reverse shocks. The principal model parameters are:  $t = 1620$  yr,  $D = 1.5$  kpc,  $n_H = 0.02$  cm $^{-3}$ ,  $E_{SN} = 1.25 \cdot 10^{51}$  erg,  $M_{ej} = 0.82 M_\odot$ ,  $M_A^b = 23$ ,  $M_A^f = 69$ ,  $\xi_0 = 0.1$ ,  $K_{ep}^f = 2.0 \cdot 10^{-2}$ ,  $K_{ep}^b = 6.8 \cdot 10^{-2}$ . The calculations lead to the following values of the magnetic fields and the shock speeds at the present epoch: the magnetic field downstream of the forward and reverse shocks  $B_f = 17.5$   $\mu$ G and  $B_b = 13$   $\mu$ G, respectively, the speed of the forward shock  $V_f = 3870$  km s $^{-1}$ , the speed of the reverse shock  $V_b = -1290$  km s $^{-1}$ .

the key parameters in order to achieve the good feet. The shock speed is related with a remnant size at given age of the remnant. This explains a slight difference of the assumed value of distances.

The results are shown in Fig.8. The magnetic fields at the reverse shock and the forward shock are comparable in this case. The energy of cosmic rays is only 10% of the explosion energy. The cosmic ray pressure at the forward shock is only 2% of the ram pressure  $\rho_0 \dot{R}_f^2$ . The particles are mainly accelerated at the reverse shock. The maximum energies are 55 TeV and 36 TeV for protons and electrons respectively. The reverse shock produces 16 % of X-ray emission.

For completeness we also consider the case when both forward and reverse shocks are not modified. The injection efficiency  $\eta_b = \eta_f = 10^{-5}$  is used. The results are shown in Fig. 9. The energy of cosmic rays is 3% of the explosion energy. The reverse shock produces 20% of X-ray emission.

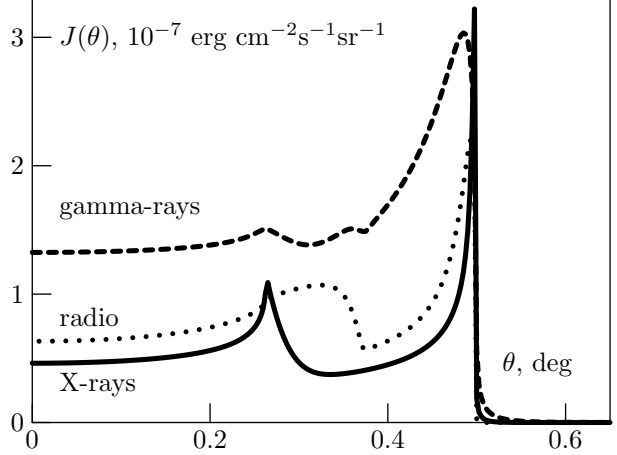


Fig. 10.— Radial profiles of 2 keV X-rays (multiplied to 0.04, solid line), 1 TeV gamma-ray emission (dashed line) and 1.4 GHz radio-emission (multiplied to  $10^3$ , dotted line), calculated for the hadronic scenario in the uniform medium.

## 6. Radial profiles

The radial profiles of brightness distributions of X-ray, gamma-ray and radio- emissions calculated for leptonic and hadronic models are shown in Fig.10-12. The projection effect is taken into account.

For the hadronic scenario in the uniform medium, all three components of radiation in the radio, X-ray and gamma-ray bands peak at the forward shock (approximately  $0.5^\circ$  of the angular radius). Note that the synchrotron emission has a sharper feature at the forward shock than the gamma-ray emission. The synchrotron emission also shows a noticeable peak at the reverse shock (approximately  $1/3$  of the brightness at the forward shock). The slight feature of gamma-rays (at the level of 10 %) at the reverse shock is due to the IC gamma-rays. The middle peak of X-ray emission in Fig. 11 is explained by the electrons accelerated at the forward shock and reaching the contact discontinuity with a stronger magnetic field. In Fig. 13 the calculated gamma-ray profiles are compared with the HESS data.

The most prominent feature at all X-ray radial profiles from Figs. 10-12 is a clear visible filament at the reverse shock. Note that the projection effect works differently for reverse shock in comparison with the forward shock (see Appendix D). As a result, at the reverse shock, the filaments are visible even in the relatively weak magnetic fields ( $13\text{--}30 \mu\text{G}$ ). Such filaments have been indeed observed by Chandra in the inner rim (Uchiyama et al. 2003, Lazendic et al. 2004).

The scale  $l_d$  of an exponential decrease of the synchrotron emissivity downstream of the shock with a velocity  $V_s$  is given by (Zirakashvili & Aharonian 2007)

$$l_d = \frac{1.4 \cdot 10^{17} \text{ cm}}{\sqrt{1 + \kappa^{1/2}}} \eta_B^{1/4} \left( \frac{V_s}{3 \cdot 10^3 \text{ km s}^{-1}} \right)^{1/2} \times \left( \frac{B_d}{100 \mu\text{G}} \right)^{-3/2} \left( \frac{\hbar \omega}{1 \text{ keV}} \right)^{-1/4}. \quad (11)$$

Here  $\kappa = B_u/B_d$  is the ratio of magnetic fields upstream and downstream of the shock. The only available profile of the linear filament in the inner region is given by Lazendic et al. 2004. Note that the profile is probably slightly influenced by CCD

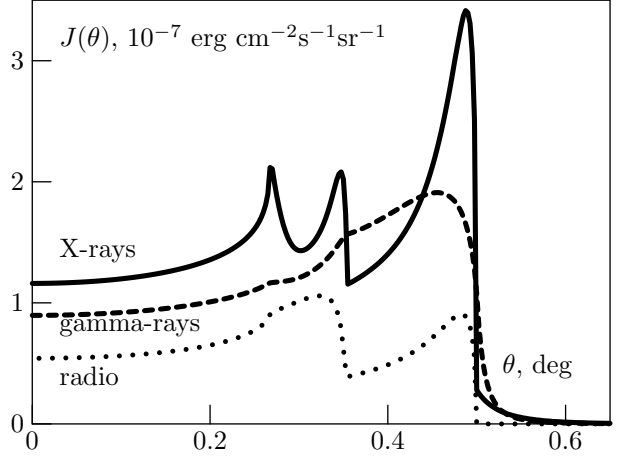


Fig. 11.— Profiles of 2 keV X-ray emission (multiplied to 0.1, solid line), 1 TeV gamma-emission (dashed line) and 1.4 GHz radio-emission (multiplied to  $10^3$ , dotted line) for the leptonic scenario with the non-modified forward shock.

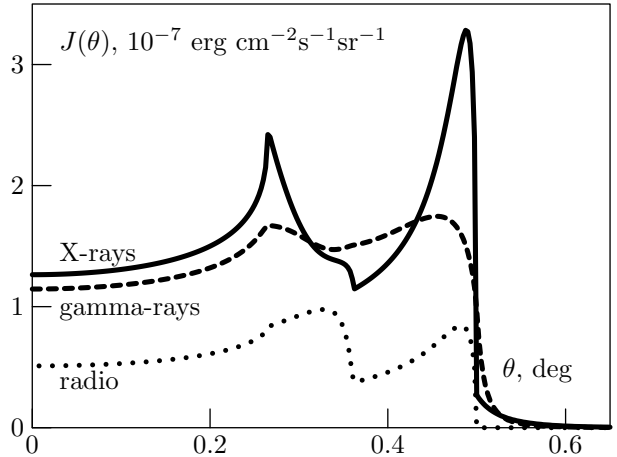


Fig. 12.— Radial profiles of 2 keV X-rays (multiplied to 0.1, solid line), 1 TeV gamma-ray emission (dashed line) and 1.4 GHz radio-emission (multiplied to  $10^3$ , dotted line) for the leptonic scenario with the non-modified forward and reverse shocks.

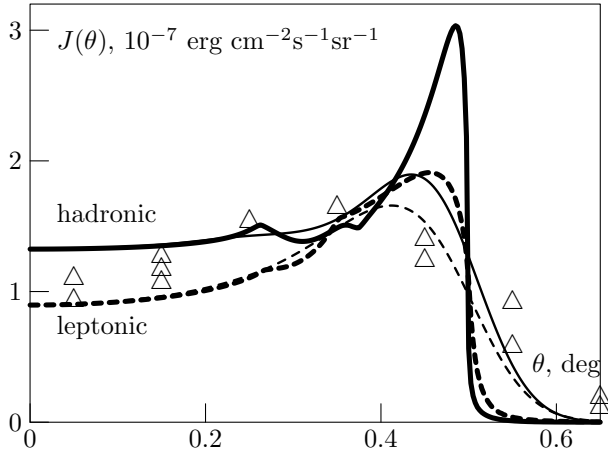


Fig. 13.— Radial Profiles of 1 TeV gamma-rays for the hadronic scenario in the uniform medium (solid) and for the leptonic scenario with the unmodified forward shock (dashed). The profiles smoothed with a Gaussian point spread function with  $\sigma = 0.05^\circ$  are also shown (thin lines). The triangles show the azimuthally averaged TeV gamma-ray radial profile observed by HESS (Aharonian et al. 2007a).

gap of Chandra. The filament width at the half of magnitude is about  $40''$ . This corresponds to  $30''$  for the exponential scale (see Appendix D) or  $l_d = 7 \cdot 10^{17}$  cm at  $D = 1.5$  kpc. Using the last formula we find  $B_d = 25 \mu G$ . So the magnetic field at the reverse shock in our calculations corresponds to the width of X-ray filaments. According to Fig.10, filaments with a similar width must be also observed at the outer X-rims in the hadronic model.

## 7. Maximum energies and magnetic amplification at the reverse and forward shocks of SNR

According to Zirakashvili & Ptuskin (2008) the maximum energy of protons  $E_m$  accelerated at the quasi-parallel shock moving in the circumstellar medium with the magnetic field strength  $B_0$  and Alfvén velocity  $V_a = B_0/\sqrt{4\pi\rho_0}$  may be found from the expression

$$E_m = 21 \text{ TeV} \frac{\left(\frac{\eta_{esc}}{0.05}\right) \left(\frac{V_f}{10^3 \text{ km s}^{-1}}\right)^2 n_H^{1/2} m_{exp} R_{pc}^f}{\ln\left(\frac{2B_0}{B_b}\right) - 1 + \left(2\frac{u'^4}{u_*^4} - 1\right)^{1/4}}. \quad (12)$$

Here  $\eta_{esc} = 2F_E/\rho_0 V_f^3$  is the ratio of the energy flux of run-away particles  $F_E$  to the flux of kinetic energy  $\rho_0 V_f^3/2$ ,  $B_b$  is the strength of the random magnetic field in the circumstellar medium,  $u_* = 1.73 \cdot 10^3 \text{ km s}^{-1}$ . The expansion parameter  $m_{exp}$  is determined as  $m_{exp} = d \ln R_f / d \ln t$  and is close to 0.5 in supernova remnants in the transition to the Sedov phase in the homogeneous medium. The speed  $u'$  is a so-called normalized shock velocity

$$u' = V_f \left(\frac{V_a}{10 \text{ km s}^{-1}}\right)^{-3/4} \left(\frac{\eta_{esc}}{0.05}\right)^{1/2} \quad (13)$$

Eq. (12) is derived for the diffusive shock acceleration in the presence of the non-resonant streaming instability suggested by Bell (2004). This equation is valid for  $u' > u_*$ . The maximum energy for lower velocities when the resonant instability should be taken into account is given by the same expression with the logarithm in the denominator only. The ratio  $\eta_{esc} = 0.14$  for the cosmic ray modified shock with the compression ratio  $\sigma = 6$  and the compression ratio of the thermal subshock 2.5. For magnetic field strength  $B_0 = 5 \mu G$  in the circumstellar medium,  $V_f = 2760 \text{ km s}^{-1}$  from the hadronic model (see Fig.6) and for a characteristic value of  $\ln 2B_0/B_b = 5$  we find  $u' = 1930 \text{ km s}^{-1}$  and  $E_m = 136 \text{ TeV}$ . This normalized shock velocity also determines the strength of the amplified magnetic field  $B \sim 2.5B_0 = 12.5 \mu G$  upstream of the forward shock or  $B \sim 75 \mu G$  downstream of the shock after the compression in the shock transition region.

These numbers are in a qualitative agreement with our numerical results obtained for the hadronic scenario. We found using Eq. (12) that the maximum energies are significantly (a factor of 40) lower in the leptonic scenario with the non-modified forward shock. This is because a small amount of accelerated protons. However the maximum energy is underestimated if one uses Eq. (12) for an oblique forward shock. The particles that run-away from such a shock will produce a

stronger electric current in a comparison with the quasi-parallel case. Since the maximum energy  $E_m$  is proportional to the current which drives the streaming instability this will permit to reach the maximum energy of several tens TeV for the leptonic scenario. This makes the leptonic scenario with the non-modified forward shock to be self-consistent.

The maximum energy and the strength of the amplified magnetic field at the reverse shock depend on the magnetic field of ejecta. The regular magnetic field strength  $B \sim 100$  G of the compact progenitor of Ib/c supernova with a radius  $R = 10^{12}$  cm will drop down to  $10^{-12}$  G after the homogeneous radial expansion of the ejecta up to radius  $3 \text{ pc} \sim 10^{19}$  cm. Probably inside the progenitor there exist stronger random magnetic fields of the order  $B \sim 10^4$  G. This fields will drop down to  $10^{-10}$  G after the homogeneous expansion. In the real situation the expansion is not homogeneous and the random magnetic field is stretched in the radial direction. This may additionally amplify the field by a factor of  $\sim 10$  that is the ratio of the stellar radius to the expected azimuthal inhomogeneity scale of the velocity field. This gives an upper limit  $10^{-9}$  G for the magnetic field strength of ejecta. The radial orientation of the field is favorable for the ion injection at the reverse shock.

The close value one may find in the model of magneto-rotational supernova explosion of Bisnovatyi-Kogan et al. 2008. The magnetic field is amplified in the differentially rotating iron core up to  $B \sim 10^{17}$  G after the core collapse and pushes the core material outward producing the supernova explosion. For the core radius  $10^6$  cm we found  $B \sim 10^{-9}$  G after the homogeneous expansion and  $B \sim 10^{-8}$  G after inhomogeneous expansion. We shall use this upper optimistic limit  $B_0 \sim 10^{-8}$  G for the estimate below.

In the hadronic model the reverse shock moves with the speed  $u = -4500 \text{ km s}^{-1}$  in the ejecta frame of reference. The ejecta number density  $n_H^{ej} = 9 \cdot 10^{-4} \text{ cm}^{-3}$ . Then the Alfvén velocity  $V_a = 0.67 \text{ km s}^{-1}$  and the normalized shock velocity  $u' = 5.7 \cdot 10^9 \text{ km s}^{-1}$  for  $\eta_{esc} = 0.14$ . Then we find  $E_m = 2.3 \text{ TeV}$  using Eq. (12). The magnetic amplification factor was not determined by Zirakashvili & Ptuskin 2008 for such high normalized velocities. The amplification factor is 190 for the normalized velocity  $u' = 3.9 \cdot 10^9 \text{ km s}^{-1}$ .

However we find  $B \sim 300B_0 = 3 \mu\text{G}$  after an extrapolation. So the amplified field downstream of the shock is  $B \sim 18 \mu\text{G}$ . The maximum energy and amplified magnetic field may be even higher if one takes into account that the number density of the highest energy particles is higher in comparison with what is expected at the shock with run-away particles. These particles cannot run away from the reverse shock easily because the upstream region of the reverse shock is located inside the remnant (see also bumps at the end of the spectra in Fig.3). Amplified magnetic field weakly depends on the initial seed field  $B_0$  as  $B \propto B_0^{1/4}$  while the dependence of the maximum energy is stronger  $E_m \propto B_0^{3/4}$  for small  $B_0$  (see Zirakashvili & Ptuskin 2008 for details).

We conclude that for the magnetic field strength  $B_0 \sim 10^{-8}$  G of ejecta the reverse shock may accelerate particles up to multi-TeV energies and may amplify magnetic fields up to tens of  $\mu\text{G}$  in the remnant considered.

## 8. Discussion

### 8.1. Thermal X-ray emission

The nonthermal emission of SNRs cannot be treated out of the context of thermal emission. In particular, any standard hadronic model of gamma-rays predicts heating of the gas to high temperatures with intense X-ray emission. The lack of such emission from the most pronounced TeV emitting SNR, RX J1713.7-3946, can be interpreted as an argument against the hadronic models of gamma-rays (Katz & Waxman 2008) or an evidence of extremely high efficiency of transformation of the kinetic energy of explosion to acceleration of relativistic particles (Drury et al. 2008).

Though our numerical calculation show that in the hadronic models of gamma-rays the thermal bremsstrahlung appears to be an order of magnitude below the Suzaku X-ray data (see Figs 6 and 7), the actual flux of X-ray emission in this energy range is higher due to the contribution from the line X-ray emission (see e.g. Ellison et al. 2007). The latter strongly depends on the chemical composition of the X-ray emitting plasma. For the composition similar to one observed in the Sun, the intensity of X-ray lines can significantly exceed the free-free continuum (see Ellison et al. 2007).

This means that such lines must be observed contrary to X-ray data. Based on this fact, Cassam-Chenaï et al. (2004) derived an upper limit on the ambient plasma density  $n_H \sim 0.02 \text{ cm}^{-3}$ . This value is several times lower than  $n_H \sim 0.1 \text{ cm}^{-3}$  in the hadronic models considered in this paper. A simplest explanation of this could be that chemical composition of the circumstellar gas is strongly different from the solar one e.g. due to absorption of X-ray line emitting ions by dust grains.

We should note that the thermal X-ray emission may be strongly depressed at the supernova shocks that are very strongly modified by the cosmic ray pressure when the shock compression ratio  $\sigma \gg 10$ . In this case only a small part of dissipating energy is transferred to the thermal plasma and the gas temperature may be below 0.1 keV even under the electron-ion thermal equilibrium (Drury et al. 2008). However such compression ratios are not observed in our model. The strong heating of the upstream plasma due to the damping of Alfvén waves results in the modest shock modification with  $\sigma \sim 6 - 7$ . Even if one assumes that the waves are not damped and the gas heating is negligible, the wave pressure will be high and it will also prevent the strong shock modification (see Caprioli et al. 2009 for details). Very high compression ratios are possible at radiative shocks in a high density plasma where the waves are damped and the gas loses energy radiatively.

Another possibility to explain a low thermal X-ray luminosity of the remnant is related with a nonuniform circumstellar medium. Chandra observations reveal a complex network of non-steady bright spots and filaments inside the X-ray emitting shell (Uchiyama et al. 2007). If dense filaments with a small volume factor exist already in the circumstellar medium and determine the mean density of the plasma, say  $1 \text{ cm}^{-3}$ , they will not be shocked by the SNR shock coming and the mean density of the shocked material will be rather low say  $0.01 \text{ cm}^{-3}$ . However the plasma density "seen" by TeV accelerated protons can be close to the total mean value because of the relatively fast diffusion. As a result they will be able to produce TeV gamma-ray with a flux close to the observed one. An enhanced magnetic field inside the filaments may also produce the observed X-ray variability of bright spots (Uchiyama et al. 2007).

An interesting consequence of this scenario is

that the gamma-ray intensity at low energies can be reduced because of the slow diffusion of GeV protons which prevents their effective penetration into the dense filaments. As a result, the gamma-ray spectrum due to p-p interactions can be quite similar to the IC gamma-ray spectra expected in leptonic models. This possibility makes quite difficult the identification of the origin of gamma-radiation.

It is interesting to note that the thermal X-rays produced in the gas shocked by the forward shock are rare observed in young supernova remnants. For example, the thermal X-ray emission of the supernova remnants Tycho and SN1006 is produced by shocked ejecta that is enriched by heavy elements (Cassam-Chenaï et al. 2007, 2008). In this regard the SNR RX J1713.7-3946 perhaps is not a very special example. It is at a later evolutionary phase in comparison with SNRs mentioned above, so the ejecta is situated deeply inside and has a very low density (see Fig.2). This could be the reason why the thermal X-ray emission of ejecta is not observed. On the other hand, the thermal emission from the downstream region of the forward shock is not detected similar to many other young SNRs.

The young remnant RCW 86 is well known source with thermal X-ray line emission observed from the forward shock (see Yamaguchi et al. 2008). It is interesting to note that in this remnant the chemical abundance of heavy ions downstream of the forward shock seems indeed below the solar one.

## 8.2. Energy spectra and morphology

The comparison of Figs. 6&7 with Figs. 8&9 shows that the spectral shape of gamma-emission is better reproduced in hadronic models. However the difference perhaps is not sufficient for a definite conclusion concerning the origin of gamma-radiation radiation based on the current data. The spectra predicted by two models deviate significantly at very high ( $\gg 10 \text{ TeV}$ ) and low  $\leq 10 \text{ GeV}$  energies. The first energy domain can be explored with the next generation ground-based detectors with significantly improved sensitivity compared to HESS. In particular, the confirmation of the the last spectral points above 30 TeV reported by HESS with limited statistical significance, would be a strong argument in favor of the hadronic



origin of gamma-rays. Also, the hadronic model predicts gamma-ray flux below 100 GeV at the level of  $\geq 10^{-11}$  erg/cm<sup>2</sup>s, while the IC gamma-ray flux predicted by the leptonic model around 1 GeV is closer to  $10^{-12}$  erg/cm<sup>2</sup>s. It is expected that the measurements conducted with the AGILE and Fermi telescopes will soon provide a decisive answer for the MeV/GeV flux from RXJ 1713.7-3946. The detection of a signal close to  $10^{-11}$  erg/cm<sup>2</sup>s would imply hadronic origin of radiation. On the other hand, the much lower flux would favor the IC origin of radiation but still could not reject the hadronic origin, given that gamma-rays could be produced in dense filaments. As discussed above, because of slow diffusion of low energy protons that prevents their effective penetration into the filaments, the GeV emission from p-p interactions in the dense filaments could be suppressed. This model can also give a reasonable, in our view, explanation of the lack of thermal X-ray line emission.

We should note, however, that the real picture could be more complex, in particular we may expect non-negligible deviations of energy spectra because of non-spherical geometry, different shock properties at different parts of the shock surface, *etc.* Moreover, one may expect comparable contributions of gamma-rays from interactions of both accelerated protons and electrons, but produced in different proportions in different regions of the remnant (see below). In this regard, detailed spectroscopic measurements of gamma-rays from different parts of the remnant seem to be a key towards understanding of acceleration processes which take place in this source.

If the magnetic field is indeed as high as required in hadronic models, we should expect, according to Fig.10, thin filaments with a width of about 30'' in the remnant periphery. The linear filaments are indeed present at Chandra image (Uchiyama et al. 2003, Lazendic et al. 2004) but in the vicinity of the inner ring that might be related to the reverse shock. This agrees with Fig.10-12. The most recent X-ray image of XMM-Newton (Acero et al. 2009) shows several linear filaments with the width 1–2' present in this image, but they all are situated inside the boundary of the X-ray emission. The boundary itself is not sharp that is presumably related with a nonuniform circumstellar medium. The lack of sharp X-

ray boundary is better explained by leptonic models. According to Fig.11 and Fig.12 some amount of X-rays is expected from the region located beyond the forward shock. In the leptonic model it is possible because accelerated electrons have sufficiently high energies to produce synchrotron X-rays in the low magnetic field.

The gamma-ray radial distributions predicted by hadronic models are sharper than the distributions calculated within the leptonic models (see Fig.13). However, because of limited angular resolution of gamma-ray telescopes, it is not possible, unfortunately, to distinguish between the distributions predicted by two models. It is demonstrated in Fig.13 in which the profiles are smoothed with a typical for Cherenkov telescope arrays point spread function assuming Gaussian distribution with  $\sigma = 0.05^\circ$ . Both smoothed profiles reasonably agree with the angular distribution of TeV gamma-rays as measured by HESS. An improvement of the angular resolution of future detectors by a factor of two should allow identification of the origin of the parent particles. On the other hand, this can be done with current detectors like HESS, VERITAS and MAGIC, for a young nearby SNR with a larger angular size. In this regard, the young supernova remnant Vela Jr (RX J0852.0-4622) with gamma-ray properties quite similar to RX J1713.7-3946 as reported by HESS (Aharonian et al. 2007b), but with angular diameter  $\approx 1^\circ$ , is a promising object for such studies.

### 8.3. Shocked clouds in the shell?

The observed ratio of the forward shock radius to the reverse shock radius robustly constraints the type of supernova explosion that produced SNR RX J1713.7-3946. For reasonable values of the energy of supernova explosion  $E_{SN} < 3 \cdot 10^{51}$  erg, the ejecta mass must be small,  $M_{ej} < 2M_\odot$ , otherwise the forward shock speed would be too low for production of synchrotron radiation extended to hard X-ray domain. Such small ejecta masses correspond to Ib/c or IIb core collapse supernova (Chevalier 2005). Circumstellar medium around these types of supernova is created by the stellar wind of the supernova progenitor. It may be a low density ( $n_H \sim 0.01$  cm<sup>-3</sup>) bubble created by stellar wind of progenitor during the main sequence period of the star evolution or by a stellar wind of a Wolf-Rayet progenitor. Because of

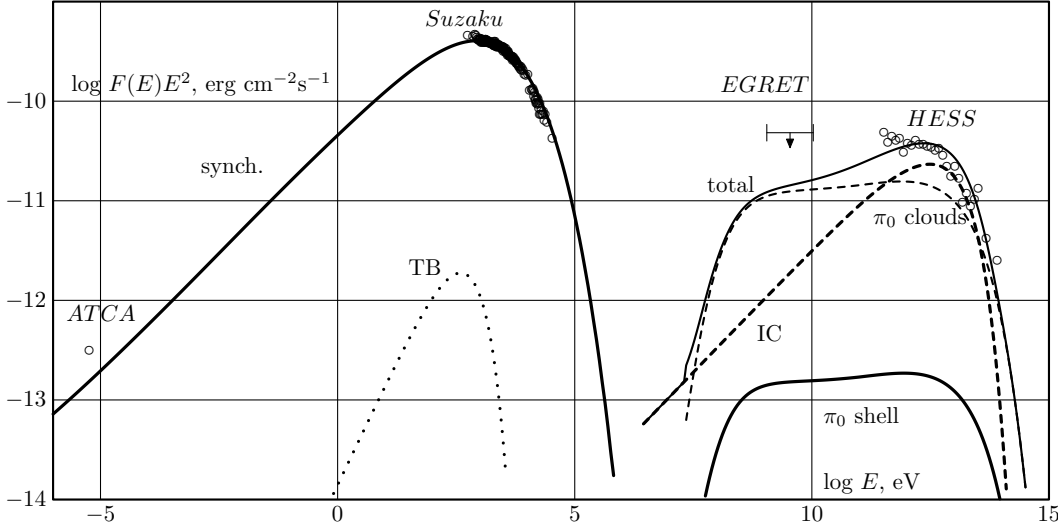


Fig. 14.— Broad-band emission of RX J1713.7-3946 for the composite scenario of gamma-rays with a non-modified forward shock and dense clouds. The principal model parameters are:  $t = 1620$  yr,  $D = 1.5$  kpc,  $n_H = 0.02$  cm $^{-3}$ ,  $E_{SN} = 1.2 \cdot 10^{51}$  erg,  $M_{ej} = 0.74 M_{\odot}$ ,  $M_A^f = 55$ ,  $M_A^b = 10$ ,  $\xi_0 = 0.1$ ,  $K_{ep}^f = 1.4 \cdot 10^{-2}$ ,  $K_{ep}^b = 9 \cdot 10^{-4}$ . The calculations lead to the following values of the magnetic fields and the shock speeds at the present epoch: the magnetic field downstream of the forward and reverse shocks  $B_f = 22$   $\mu$ G and  $B_b = 31$   $\mu$ G, respectively, the speed of the forward shock  $V_f = 3830$  km s $^{-1}$ , the speed of the reverse shock  $V_b = -1220$  km s $^{-1}$ . The following radiation processes are taken into account: synchrotron radiation of accelerated electrons (solid curve on the left), thermal bremsstrahlung (dotted line), IC gamma-ray emission of the entire remnant including forward and reverse shocks (dashed line), hadronic component of gamma-rays from the remnant's shell (solid line on the right) as well as from dense clouds assuming the factor of 120 enhancement of the flux (thin dashed line). We also show the total gamma-ray emission from the entire remnant including the dense clouds (thin solid line).

very low densities, the observed gamma-rays can be produced only via IC scattering of electrons. If the bubble is created during the Red Supergiant stage of the supernova progenitor or during the interaction of the slow Red Supergiant wind with the fast Wolf-Rayet wind, the gas density could be sufficiently high for effective production of gamma-rays at interactions of accelerated protons.

In all models considered the forward shock of SNR have swept only  $6-15 M_{\odot}$ . This mass is comparable or slightly less than the mass ejected by progenitors of Ib/c and IIb supernova during the stellar evolution. This means that the shock just have swept the progenitor's material ejected during the stellar evolution. The interaction with the molecular gas surrounding the remnant only starts. The exceptions could be the very dense cores of molecular gas (clouds C and D) that are situated already inside the forward shock (Fukui

2008). Probably the forward shock has enveloped the clouds, and a high pressure gas from the downstream region drove secondary shocks into the clouds (see Chevalier 1977 for a review). These shocks are strongly decelerated and become radiative. That is why they do not produce the thermal X-rays (see also Cassam-Chenaï et al. 2004). The nonthermal X-rays can be produced at these shocks by high-energy electrons from the remnant's shell in the compressed magnetic field of the cloud, while the highest energy gamma-rays from pion decay are mainly produced inside the cloud where the target density is high (Fukui 2008).

If the highest energy protons freely penetrate into the clouds, the corresponding gamma-emission from the pion decay may exceed the gamma-emission from the pion decay of the remnant by a factor that is the ratio of the cloud mass to the mass swept up by the forward shock. If the

clouds C and D indeed contain about 100-1000 solar masses (Fukui 2008), this ratio should be close to 10-100. Since this is not the case, as it follows from the HESS results, the hadronic models can survive only if the penetration into the clouds is depressed. Such a possibility seems unlikely, at least for the highest energy protons.

On the other hand, in the leptonic models of gamma-rays, in which the bulk of the gamma-ray emission is produced via IC scattering of electrons, one may expect significant contribution of hadronic gamma-rays produced in the clouds C and D. Namely the gamma-ray fluxes from p-p interactions shown in Figs.8&9 can be enhanced by 1 or 2 orders of magnitude. Apparently, from these regions we should expect also low energy, MeV/GeV gamma-rays. Because of low density of the ambient gas, the gamma-radiation outside the C and D clouds will be dominated by the IC component, therefore the gamma-ray flux at MeV/GeV energies is expected to be faint (see Figs.8.&9).

In Fig. 14 we demonstrate the feasibility of the "composite" scenario. The hadronic component of gamma-rays from dense clouds is shown by multiplying the flux expected from the low density gas downstream of the forward shock by a factor of 120. The ratio of the gamma-rays from clouds to the flux from other parts of the shell depends on the ratio of the mass of clouds to the mass of the shell, provided that all particles freely enter the dense clouds. This however could not be the case especially for the low energy particles which introduces large uncertainties in the predictions of the flux of this component of radiation. On the other hand, if the enhancement of hadronic gamma-rays in clouds is indeed very large, this could help to improve the fit of the gamma-ray data both at low (sub TeV) and high energy (multi-TeV) regions (see Fig. 14). Note that in this scenario we expect also gamma-rays from dense clouds due to bremsstrahlung of electrons. However, as long as the total energy in protons significantly exceeds the energy in relativistic electrons, the interaction of latters with the dense gas will dominate over the bremsstrahlung.

#### 8.4. Reverse shock in hadronic and leptonic models

The parameters characterizing acceleration of particles in the reverse shock in the leptonic models are not strongly constrained. While in the hadronic models the reverse shock must be an efficient accelerator of multi TeV electrons in order to produce the synchrotron X-radiation observed from the inner ring, in the leptonic models the acceleration by the inverse shock is not required. Indeed, in the leptonic models the electrons accelerated at the forward shock may easily reach the contact discontinuity downstream of the forward shock with relatively weak magnetic fields. They will produce X-rays in the amplified magnetic field between the contact discontinuity and the reverse shock (see Fig.11). The magnetic field cannot be weak in this region since the inner ring is clearly visible in radio. The corresponding radio-electrons must be accelerated at the reverse shock. The magnetic field amplified at the reverse shock has probably rather small scales. This is because the scale of the most unstable MHD mode is proportional to the strength of the undisturbed field in the case of the non-resonant streaming instability (Bell 2004).

The magnetic field of ejecta  $B < 10^{-8}$ G is significantly smaller than the field in the circumstellar medium (presumably about  $10^{-6}$  G). The small-scale magnetic field is not a very efficient scatter of highest energy electrons. As a result, the diffusion may be significantly faster than the Bohm diffusion, and the acceleration at the reverse shock up to TeV energies might be impossible. However, acceleration of GeV electrons producing synchrotron radio emission is quite probable. On the other hand, if the reverse shock is an effective accelerator, it may produce the additional component(s) of nonthermal radiation. For example, in the case of weak magnetic fields at the reverse shock, the hadronic models may result in detectable IC gamma-rays from the central region of the remnant. Probably the situation is different in the remnant Cas A, where the magnetic field at the reverse shock is stronger than the magnetic field at the forward shock. This may be related with a different acceleration efficiency of the shocks in the remnant Cas A. For example, the reverse shock may be modified and the forward shock not. The reverse shock energetics in Cas A

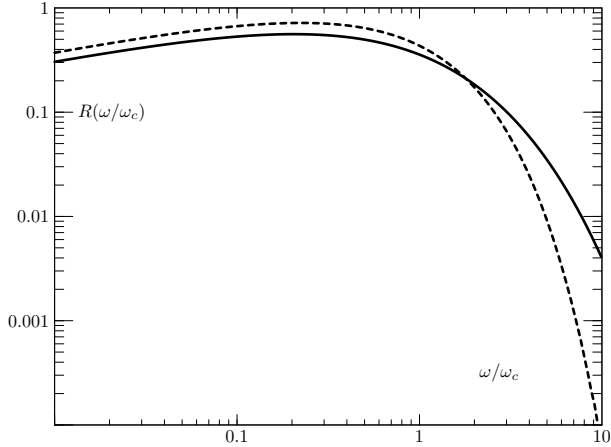


Fig. 15.— The synchrotron emissivity of a single electron in the isotropic magnetic field. The function  $R(x)$  for single value of the magnetic field strength given by Eq.(A2) (dashed line) and the function  $R_1(x)$  (solid line) given by Eq. (A5) are shown.

is of the order of 10 % from the total one. It is enough to explain the observable TeV gamma-rays in the framework of hadronic models.

## 9. Conclusion

Our study of the nonlinear diffusive shock acceleration in RX J1713.7-3946, and calculations of the related electromagnetic radiation lead to the following conclusions:

1. The present reverse shock position may be reproduced if the SNR RX J1713.7-3946 is the remnant of Ib/c or IIb type supernova with the ejected mass  $M_{ej} < 2M_{\odot}$ .

2. The available radio, X-ray and gamma-ray data can be explained by both the leptonic and hadronic models, although with certain caveats. The spectral shape of gamma-emission is better reproduced in hadronic models. The morphology of electromagnetic emission in X-ray and TeV gamma-ray bands can be in principle reproduced by both the hadronic and leptonic models.

3. The hadronic origin is possible only if the following conditions are satisfied:

- a) The forward shock is strongly modified throughout all surface.
- b) Chemical abundance of heavy ions in X-ray emitting regions should be significantly below the

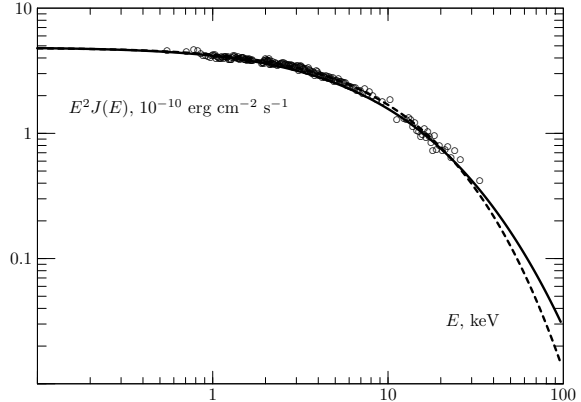


Fig. 16.— Spectra of synchrotron X-rays produced at the shock with a distributed magnetic field (Eq. (B5), solid line) and at the shock with a single-valued magnetic field (Eq.(B3), dashed line). Suzaku data (circles) for the remnant RX J1713.7-3946 are also shown.

solar one.

- c) The lack of the predicted by hadronic models sharp outer X-ray rim can be explained by the nonuniform circumstellar medium.

- d) If the forward shock interacts with clouds D and C, the penetration of the highest energy protons into the clouds must be suppressed.

4. Any detection of GeV gamma-rays by AGILE and Fermi satellites at the level of  $F \geq 10^{-11}$  erg cm $^{-2}$  s $^{-1}$ , especially outside the dense clouds C and D, would be a decisive argument in favor of the hadronic origin of TeV gamma-rays. The leptonic models predict very hard energy spectra of gamma-rays with absolute energy fluxes as low as  $F = 2 \cdot 10^{-12}$  erg cm $^{-2}$  s $^{-1}$ . However a low flux and hard gamma-ray spectrum are expected also in the hadronic models with dense filaments, assuming energy-dependent cosmic ray penetration into the clouds.

5. The leptonic models imply that the bulk of the observed gamma-radiation is produced via IC scattering of electrons. However, these models allow also significant contributions of hadronic gamma-rays from dense gas region in the shell, in particular from the clouds C and D. In such "composite" models we should expect relatively high fluxes of low energy gamma-rays from the C and D clouds, while outside these condensations the MeV/GeV flux is expected to be quite low.

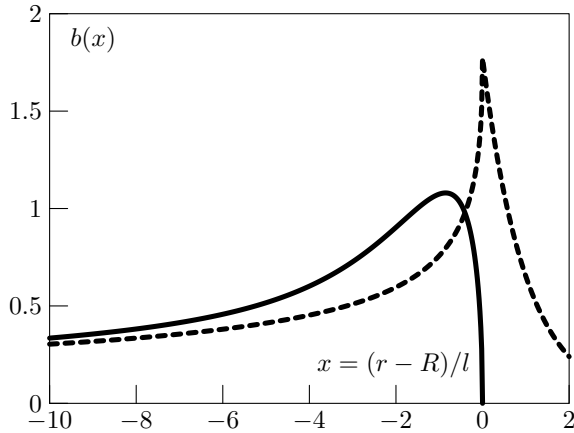


Fig. 17.— The function  $b(x)$  that describes the radial profile of the X-ray brightness for the forward shock (Eq. (D2), solid line) and for the reverse shock (Eq.(D3), dashed line).

6. If the inner ring of RX J1713.7-3946 is indeed produced by the reverse shock, its proper motion can be measured. X-ray data of Chandra may be used for this purpose since the X-ray filaments in the inner ring region have been observed (Lazendic et al. 2004, Uchiyama et al. 2003). In all models considered the reverse shock moves with several thousand kilometers per second to the center of the remnant. The model with  $r^2$  density profile has the highest absolute value of the reverse shock speed,  $V_b = -3010 \text{ km s}^{-1}$  or even larger for a sharper density profile. The measurement of the reverse shock speed will constrain the gas density distribution around this SNR.

We thank T. Tanaka for providing us with the Suzaku X-ray data. We are grateful to H. Völk for the useful discussions on cosmic ray acceleration in SNRs. VNZ acknowledge the hospitality of the Max-Planck-Institut für Kernphysik, where the major part of this work was carried out. The work of VNZ was also supported by the RFBR grant in Troitsk.

### A. Synchrotron emission in the turbulent medium

The synchrotron emissivity in the medium with nonuniform magnetic field can be written as

$$\epsilon(\omega) = \frac{\sqrt{3}q^3}{2\pi m_e c^2} \int dB B P(B) \int p^2 dp N(p) R(\omega/\omega_c) \quad (\text{A1})$$

where  $\omega_c$  is the characteristic frequency of synchrotron radiation  $\omega_c = 1.5 q B p^2 / m_e^3 c^3$ . The function  $P(B)$  is the probability distribution of the magnetic field. If the magnetic field strength has a single value  $B_0$ , then  $P(B) = \delta(B - B_0)$  and this equation is reduced to a standard formula for the synchrotron emissivity.

The function  $R(x)$  of the argument  $x = \omega/\omega_c$  describes synchrotron radiation of a single electron in magnetic field with chaotic directions. Crusius & Schlickeiser (1986) derived an exact expression for  $R(\omega/\omega_c)$  in terms of Whittaker's function. With an accuracy of several percent  $R(\omega/\omega_c)$  can be presented in a simple analytical form (Zirakashvili & Aharonian 2007):

$$R(x) = \frac{1.81 \exp(-x)}{\sqrt{x^{-2/3} + (3.62/\pi)^2}}. \quad (\text{A2})$$

In the turbulent medium the magnetic field is not uniform and is described by a probability distribution  $P(B)$ . It reveals the exponential tails when the magnetic field is amplified by turbulent motions (see Schekochihin et al. 2004). The probability distribution found in the numerical simulations of the nonresonant streaming instability may be written in the simple analytical form (Zirakashvili & Ptuskin 2008):

$$P(B) = \frac{6B}{B_{rms}^2} \exp(-\sqrt{6}B/B_{rms}). \quad (\text{A3})$$

Here  $B_{rms} = \langle B^2 \rangle^{1/2}$  is the square root of the mean square of the random magnetic field (note the corrected missprint in the normalization factor in this equation). Now the synchrotron emission of a single electron is described by the function  $R_1(x)$ :

$$R_1(x) = 6 \int_0^\infty dy y^2 R(x/y) \exp(-\sqrt{6}y). \quad (\text{A4})$$

We found a useful analytical approximation of this function

$$R_1(x) = 1.50x^{1/3} \left(1 + 1.53x^{1/2}\right)^{11/6} \exp\left(-96^{1/4}x^{1/2}\right) \quad (\text{A5})$$

The functions  $R(x)$  and  $R_1(x)$  are shown in Fig. (15).

Qualitatively similar results were found by Bykov et al. 2008, but assuming Gaussian probability distribution for  $P(B)$ .

### B. Analytical expressions for the synchrotron X-rays

The analytical approximations for the electron and synchrotron spectra at the non-modified shock were found by Zirakashvili & Aharonian 2007. The synchrotron loss dominated regime was considered. In the case of the single valued magnetic field the synchrotron spectra are parameterized with the principal parameter  $E_0$ :

$$E_0 = \frac{81}{64(1 + \kappa^{1/2})^2} \frac{\hbar m_e c V_f^2}{q^2 \eta_B} = \frac{2.2 \text{ keV}}{(1 + \kappa^{1/2})^2 \eta_B} \left( \frac{V_f}{3 \cdot 10^3 \text{ km s}^{-1}} \right)^2. \quad (\text{B1})$$

Here  $\kappa$  is the ratio of the upstream and downstream magnetic field strength. In the case when magnetic field has the same value upstream and downstream of the shock ( $\kappa = 1$ ) the spectrum of synchrotron X-rays has the following form

$$F(E) \propto E^{-2} \left[ 1 + 0.46 \left( \frac{E}{E_0} \right)^{0.6} \right]^{11/4.8} \exp \left( -\sqrt{\frac{E}{E_0}} \right) \quad (\text{B2})$$

In the case when ratio of the upstream and downstream magnetic field strength  $\kappa = 1/\sqrt{11}$ , the spectrum of synchrotron X-rays is mainly determined by the downstream region and has the following form

$$F(E) \propto E^{-2} \left[ 1 + 0.38 \left( \frac{E}{E_0} \right)^{0.5} \right]^{11/4} \exp \left( -\sqrt{\frac{E}{E_0}} \right). \quad (\text{B3})$$

Suzaku data obtained for RX J1713.7-3946 in a broad energy interval from 0.4 to 40 keV are well fitted by these spectra (Uchiyama et al. 2007, Tanaka et al. 2008). For example,  $E_0 \approx 0.94$  keV for Eq.(B3).

In the case of distributed magnetic field one should use Eq.(A5) instead of Eq.(A2). Using the electron spectra of Zirakashvili & Aharonian 2007 we found the following synchrotron spectra

$$F(E) \propto E^{-2} \left[ 1 + 0.172 \left( \frac{E}{E_1} \right)^{0.46} \right]^{25/(12 \cdot 0.46)} \exp \left[ - \left( \frac{E}{E_1} \right)^{1/3} \right], \quad \kappa = 1, \quad (\text{B4})$$

and

$$F(E) \propto E^{-2} \left[ 1 + 0.185 \left( \frac{E}{E_1} \right)^{0.4} \right]^{25/(12 \cdot 0.4)} \exp \left[ - \left( \frac{E}{E_1} \right)^{1/3} \right], \quad \kappa = 1/\sqrt{11}. \quad (\text{B5})$$

Here the parameter  $E_1$  is

$$E_1 = \frac{\sqrt{6}}{128(1 + \kappa^{1/2})^2} \frac{\hbar m_e c V_f^2}{q^2 \eta_B} = \frac{0.134 \text{ keV}}{(1 + \kappa^{1/2})^2 \eta_B} \left( \frac{V_f}{3 \cdot 10^3 \text{ km s}^{-1}} \right)^2. \quad (\text{B6})$$

Suzaku data may be fitted with  $E_1 \approx 0.036$  keV using the formula (B5). This value and  $\eta_B = 2$  corresponds to the shock velocity  $V_f = 3300 \text{ km s}^{-1}$ . This number is slightly above the corresponding values in the hadronic scenario when the larger compression ratio of the modified shocks and the additional input of the faster reverse shock should be taken into account. The shock velocity is higher in the leptonic scenario when the adiabatic losses downstream of the shock play a role.

The spectra given by Eqs.(B3),(B5) and Suzaku data are shown in Fig.16. The distributed magnetic field makes the cut-off of synchrotron spectra slightly smoother in comparison with a single-value case. The cut-off energy is a factor of 1.6 higher for the distributed magnetic field.

The spectrum (B5) shows a rather slow drop beyond the cut-off. It may be used for explanation of the high-energy X-ray tail observed in the supernova remnant Cas A.

### C. Simple estimates of the gamma-ray emission and thermal X-ray emission in SNR.

Using Eq. (10) one can estimate the characteristic electron temperature downstream of the forward shock. Assuming a linear radial profile of the gas velocity we found the following expression for the maximum electron temperature

$$T_e = \left( \xi_g (n_H + 4n_{He}) \lambda_{ep} R V_f \frac{4\sigma\sqrt{2m_e} q^4}{3(\sigma-1)m} \right)^{2/5} = 1.6 \text{keV } n_H^{2/5} \left( \frac{\sigma \xi_g}{\sigma-1} \right)^{2/5} \left( \frac{R_f}{3 \text{ pc}} \right)^{2/5} \left( \frac{V_f}{3 \cdot 10^3 \text{ km s}^{-1}} \right)^{2/5} \quad (\text{C1})$$

Here  $\xi_g = P_g / \rho_0 V_f^2$  is the ratio of the gas pressure downstream the shock  $P_g$  to the dynamical pressure  $\rho_0 V_f^2$  and  $\sigma$  is the total compression ratio of the shock. The time derivative of the temperature was neglected in Eq.(10). For cosmic ray modified shock in the hadronic model  $\xi_g \sim 0.25$ ,  $\sigma = 6.5$  and we obtain  $T_e = 0.6$  keV in agreement with the numerical results.

It is clear from Eq.(C1) that the dependence of the electron temperature on the shock parameters is rather weak. E.g at the Sedov stage  $T_e \propto t^{-0.08}$ . It also weakly (only a factor of 2) affected by the shock modification. Note that the electron-ion equilibration case when the electron temperature  $T_e \propto V_f^2$  and may be strongly reduced by the shock modification (see e.g. Drury et al. 2008).

X-ray emissivity due to the thermal bremsstrahlung is given by (Rybicki & Lightman 1979)

$$E^2 \epsilon_{ff} = \frac{8q^6}{3m_e c^3 h} \left( \frac{2\pi}{3m_e T_e} \right)^{1/2} E \sum_i Z^2 n_e n_i \tilde{g}_{ff} \exp \left( -\frac{E}{T_e} \right). \quad (\text{C2})$$

Here  $Z$  is the charge number of plasma ions,  $\tilde{g} \sim 1$  is the Gount factor. Assuming the radial density profile downstream of the shock  $\rho \propto r^{3(\sigma-1)}$  and the uniform electron temperature we find the flux of the thermal X-rays

$$E^2 F_X = \frac{\sigma^2}{6\sigma-3} \frac{8q^6}{3m_e c^3 h} \left( \frac{2\pi}{3m_e T_e} \right)^{1/2} \left( 1 + 2 \frac{n_{He}}{n_H} \right) \left( 1 + 4 \frac{n_{He}}{n_H} \right) \frac{n_H^2 R_f^3}{D^2} \frac{E}{T_e} \exp \left( -\frac{E}{T_e} \right) \tilde{g}_{ff} = \\ 2.5 \cdot 10^{-11} \frac{\text{erg}}{\text{s cm}^2} \frac{\sigma^2}{6\sigma-3} n_H^2 R_{pc}^3 D_{kpc}^{-2} T_{keV}^{1/2} \frac{E}{T_e} \exp \left( -\frac{E}{T_e} \right). \quad (\text{C3})$$

The gamma-ray flux from the pion decay at energies below the cut-off may be estimated as (e.g. Zirakashvili 2008)

$$E^2 F_{pp}(E) = \frac{R_f^3 K_{\pi\pi} \sigma_{pp} c n_H^2 \xi_{cr} m V_f^2}{D^2 \ln(p_{\max}/mc)} \left( 1 + 4 \frac{n_{He}}{n_H} \right)^2 = 1.6 \cdot 10^{-11} \frac{\text{erg}}{\text{s cm}^2} \xi_{cr} R_{pc}^3 D_{kpc}^{-2} n_H^2 \left( \frac{V_f}{3 \cdot 10^3 \text{ km s}^{-1}} \right)^2 \quad (\text{C4})$$

Here  $K_{\pi\pi} = 0.17$  is the fraction of the proton energy transmitted to the parent neutral pions,  $\sigma_{pp}$  is the total inelastic  $p-p$  cross-section,  $p_{\max}$  is the maximum momentum of accelerated protons and  $\xi_{cr}$  is the ratio of the cosmic ray pressure downstream of the shock  $P_{cr}$  to the dynamical pressure  $\rho_0 V_f^2$ . We use the value  $\sigma_{pp} = 4 \cdot 10^{-26}$  for this estimate of the flux of TeV gamma-rays. It was assumed that the accelerated protons with power-law  $E^{-2}$  distribution fill the remnant uniformly.

The intensity of gamma-rays from the IC scattering in the synchrotron losses dominated case may be estimated as (Zirakashvili 2008)

$$E^2 F_{IC} = \frac{3\xi_{cr}}{8\xi_B} \frac{K_{ep} R_f^2 U_{rad} V_f}{D^2 \ln(p_{\max}/mc)} = 9 \cdot 10^{-12} \frac{\text{erg}}{\text{s cm}^2} R_\theta^2(\text{deg}) \frac{V_f}{3 \cdot 10^3 \text{ km s}^{-1}} \frac{K_{ep}}{10^{-2}} \frac{\xi_{cr}}{\xi_B} \frac{U_{rad}}{4 \cdot 10^{-13} \text{ erg cm}^{-3}} \quad (\text{C5})$$

Here  $\xi_B$  is the ratio of the magnetic energy  $B^2/8\pi$  to the dynamical pressure  $\rho_0 V_f^2$ ,  $U_{rad}$  is the energy density of the scattered photons and  $R_\theta(\text{deg})$  is the angular radius of the shock in degrees.



The ratio of the gamma-ray energy flux to the thermal bremsstrahlung energy flux at its maximum at  $E_X = T_e$  is given by equation (see also Katz & Waxman 2008)

$$\frac{E^2 F_{pp}}{E_X^2 F_X} = 1.7 \xi_{cr} \frac{6\sigma - 3}{\sigma^2 T_{keV}^{1/2}} \left( \frac{V_f}{3 \cdot 10^3 \text{ km s}^{-1}} \right)^2 \quad (\text{C6})$$

These fluxes are comparable for cosmic-ray modified shocks with  $\xi_{cr} \sim 0.5$  and  $\sigma \sim 6$ .

#### D. Projection effect for a forward and a reverse shock

The surface brightness  $J$  is determined by the integral of emissivity  $\epsilon$  along the line of sight. For spherically symmetric case it can be written as

$$J(r) = 2 \int_r^\infty \frac{r' dr' \epsilon(r')}{\sqrt{r'^2 - r^2}} \quad (\text{D1})$$

For a forward shock the emissivity downstream can be written as  $\epsilon = \epsilon_0 H(R - r) \exp((r - R)/l)$ . Here  $H(r)$  is the step function. For a reverse shock the emissivity has the form  $\epsilon = \epsilon_0 H(r - R) \exp((R - r)/l)$ . For a thin shell of X-ray emission  $l \ll R$  the surface brightness  $J(r) = \sqrt{2Rl} \epsilon_0 b(x)$  may be written in terms of the function  $b(x)$  of argument  $x = (r - R)/l$ .

For the forward shock this function (see also Ballet 2006)

$$b(x) = \begin{cases} 2 \exp(x) \int_0^{\sqrt{-x}} dy \exp(y^2), & x < 0 \\ 0, & x > 0 \end{cases} \quad (\text{D2})$$

while for the reverse shock

$$b(x) = \exp(-x) \begin{cases} 2 \int_{\sqrt{-x}}^\infty dy \exp(-y^2), & x < 0 \\ \sqrt{\pi}, & x > 0 \end{cases} \quad (\text{D3})$$

The function  $b(x)$  is shown in Fig.17. For the forward shock the function  $b(x)$  has a width  $w = 4.6l$  at the half of maximum and  $w = 7.5l$  at the  $1/e$  of maximum. These numbers are in agreement with results of Ballet 2006 and Berezhko & Völk 2004. For the reverse shock this function has a width  $w = 1.3l$  at the half of maximum and  $w = 2.6l$  at the  $1/e$  of maximum.

## REFERENCES

- Acero, F., Ballet, J., Decourchelle, A., Lemoine-Goumard, M., Ortega, V., Gianti, E., Dubner, G., & Cassam-Chenai 2009, A&A, submitted
- Aharonian, F.A., Buckley, J., Kifune, T., Sinnis, G. 2008, Rep. Prog. Phys., 71, 096901
- Aharonian F. et al. 2006, Nature, 432, 223
- Aharonian F. et al. 2006, A&A, 449, 223
- Aharonian F. et al. 2007, A&A, 464, 253
- Aharonian F. et al., 2007, ApJ, 661, 236
- Amato, E., & Blasi, P., 2006, MNRAS, 371, 1251
- Axford, W.I., Leer, E., Skadron, G., 1977, Proc. 15th Int. Cosmic Ray Conf., Plovdiv, 90, 937
- Ballet, J., 2006, Adv. in Space Res. 37, 1902
- Bell, A.R., 1978, MNRAS, 182, 147
- Bell, A.R., 2004, MNRAS, 353, 550
- Berezhko, E.G., Elshin, V.K., Ksenofontov, L.T., 1994, Astropart. Phys. 2, 215
- Berezhko, E.G., & Völk, H.J. 2004a, A&A 419, L27
- Berezhko, E.G., & Völk, H.J. 2006, A&A 451, 981
- Bisnovatyi-Kogan, G.S., Moiseenko, S.G., & Ardelyan, N.V. 2008, Astron. Reports 52, 997
- Blandford, R.D., & Ostriker, J.P. 1978, ApJ, 221, L29
- Blumenthal, G.R., & Gould, R.J., 1970, Rev. Mod. Phys. 42, 237
- Bykov, A.M., Uvarov, Yu.A., & Ellison, D., 2008, ApJ 689, L133
- Caprioli, D., Blasi, P., Amato, E., & Vietri, M., 2009, MNRAS 395, 895
- Cassam-Chenai, G., Decourchelle, A., Ballet, J., Sauvageot, J.-L., Dubner, G., & Giacani, E., 2004, A&A 427, 199
- Cassam-Chenai, G., Hughes, J.P., Ballet, J., & Decourchelle, A., 2007, ApJ 665, 315
- Cassam-Chenai, G., Hughes, J.P., Reynoso, E.M., Badenes, C., & Moffett, D., 2008, ApJ 680, 1180
- Chevalier, R., 1977, Ann. Rev. Astron. Astrophys., 15, 175
- Chevalier, R., 1982, ApJ, 258, 790
- Chevalier, R., 1982, ApJ, 259, 302
- Chevalier, R., 2005, ApJ, 619, 839
- Chevalier, R., 2006, ApJ 651, 381
- Crusius, A., & Schlickeiser, R. 1986, A&A 164, L16
- Ellison, D., Slane, P., & Gaensler, B.M., 2001, ApJ 563, 191
- Ellison, D., Decourchelle, A., & Ballet, J., 2005, A&A 429, 569
- Ellison, D., Patnaude, D.J., Slane, P., Blasi, P., & Gabici, S., 2007, ApJ 661, 879
- Drury, L.O.C., Aharonian, F.F., Malyshev, D., & Gabici, S., 2009, A&A 496, 1
- Fukui, Y., Moriguchi, Y., Tamura, K., et al., 2003, PASJ 55, L61
- Fukui, Y., 2008, Proc. of 4th International Meeting on High-Energy Gamma-Ray Astronomy, Heidelberg, Germany, 7-11 July 2008, AIP Conference Proceedings 1085, 104
- Helder, E.A., & Vink, J., 2008, ApJ 686, 1094
- Hiraga, J.S., Uchiyama, Y., Takahashi, T., & Aharonian, F.A., 2005, A&A 431, 953
- Jun, B., & Norman, M.L., 1996, ApJ 465, 800
- Kelner, S.R., Aharonian, F.A., & Bugayov, V.V., 2006, Phys. Rev. D, 74, 034018
- Kang, H., Jones, T.W., 2006, Astropart. Phys. 25, 246
- Katz, B., & Waxman, 2008, Journ. of Cosmology and Astropart. Phys., 1, 18
- Koyama, K., Kinugasa, K., Matsuzaki, K., et al., 1997, PASJ 49, L7

- Krymsky, G.F. 1977, Soviet Physics-Doklady, 22, 327
- Lagage, P.O., & Cesarsky, C.J., 1983, A&A, 118, 223
- Lazendic, J.S., Slane, P.O., Gaensler, B.M., Plucinsky, P.P., Hughes J.P., Galloway, D.K., & Crawford, F., 2004, ApJ 602, 271
- Lazendic, J.S., Slane, P.O., Gaensler, B.M., Reynolds, S.P., Plucinsky, P.P., & Hughes, J.P., 2004, ApJ 602, 271
- Malkov, M.A., & Drury, L.O’C, 2001, Reports on Progress in Physics, 64, 429
- McKenzie, J.F., & Völk, H.J., 1982, A&A, 116, 191
- Morlino, G., Amato, E., & Blasi, P., 2008, MNRAS 392, 240
- Muraishi, H., Tanimori, T., Yanagita, S. et al. 2000, A&A 354, L57
- Pfeffermann, E., & Aschenbach, B., in Röntgenstrahlung from the Universe, Ed. H.U. Zimmermann, J., J. Trümper, & H.Yorke (MPE Rep.263) 267
- Ptuskin, V.S., & Zirakashvili, V.N. 2005, A&A, 429, 755
- Schekochihin, A.A., Cowley, S.C., & Taylor, S.F., 2004, ApJ 612, 276
- Rybicki, G.B., & Lightman, A.P. 1979, Radiative Process in Astrophysics (New York: Wiley)
- Slane, P., Gaensler, B.M., Dame, T.M., et al., 1999, ApJ 525,357
- Spitzer, L. 1968, Diffuse matter in space (New York: Interscience)
- Takahashi, T., Tanaka, T., Uchiyama, Y., et al., 2008, PASJ 60S, 131
- Tanaka, T., Uchiyama, Y., Aharonian, F. et al., 2008, ApJ 685, 988
- Trac, H., Pen, U. 2003, Publ. Astron. Soc. Pacific 115, 303
- Uchiyama, Y., Aharonian, F., & Takahashi,T., 2003, A&A 400, 567
- Uchiyama, Y., Aharonian, F., Tanaka, T., Takahashi,T., & Maeda, Y., 2007, Nature 449, 576
- Vladimirov, A., Ellison, D.C., & Bykov, A., 2006, ApJ, 652, 1246
- Völk, H.J., Berezhko, E.G., & Ksenofontov, L.T., 2005, A&A, 433, 229
- Wang, Z.R., Qu, Q.Y., & Chen, Y., 1997, A&A, 318, L59
- Yamaguchi, H., Koyama, K., Nakajima, H., Bamba, A., Yamazaki, R., Vink, J., & Kawachi, A., 2009, PASJ 60, S123
- Zirakashvili, V.N. 2007, A&A 466, 1
- Zirakashvili, V.N., & Aharonian, F., 2007, A&A 456, 695
- Zirakashvili, V.N., Ptuskin, V.S., 2008, ApJ 678, 939
- Zirakashvili, V.N., 2008, Proc. of 4th International Meeting on High-Energy Gamma-Ray Astronomy, Heidelberg, Germany, 7-11 July 2008, AIP Conference Proceedings 1085, 129
- Zirakashvili, V.N., Ptuskin, V.S., 2009, in preparation